

# Analysis on the composite nature of the light scalar mesons $f_0(980)$ and $a_0(980)$

Ze-Qiang Wang<sup>1</sup>, Xian-Wei Kang<sup>1,2,\*</sup>, J. A. Oller<sup>3,†</sup> and Lu Zhang<sup>1</sup>

<sup>1</sup> *Key Laboratory of Beam Technology of Ministry of Education,*

*College of Nuclear Science and Technology,*

*Beijing Normal University,*

*Beijing 100875, China*

<sup>2</sup> *Beijing Radiation Center,*

*Beijing 100875, China*

<sup>3</sup> *Departamento de Física. Universidad de Murcia,*

*E-30071 Murcia, Spain*

We study the weight or compositeness of the  $\pi\pi-K\bar{K}$  and  $\pi\eta-K\bar{K}$  in the composition of the  $f_0(980)$  and  $a_0(980)$  resonances, respectively. Either we use the saturation of the total width and compositeness, or we use a Flatté parameterization taking also into account the spectral function of a near-threshold resonance. We make connections and compare between these two methods. We take input values for the pole mass and width from several determinations in the literature. In addition, we take as third input either the total compositeness or the decay-width branching ratio to the lighter channel for each resonance. It turns out that for the poles considered the meson-meson components are dominant for the  $f_0(980)$ , while for the  $a_0(980)$  resonance they are subdominant. We also provide partial decay widths and partial compositeness coefficients, so that the  $K\bar{K}$  component is the most important one for the  $f_0(980)$ . Additionally, this study stresses the need to distinguish between the bare and dressed couplings and widths in a Flatté parameterization. We elaborate on the connection between the partial-decay widths calculated in terms of the dressed couplings and the actual measured ones. Due to the coupled-channel dynamics when the pole lies near the heavier threshold in the second Riemann sheet some changes are needed with respect to standard relations.

---

\* [xwkang@bnu.edu.cn](mailto:xwkang@bnu.edu.cn)

† [oller@um.es](mailto:oller@um.es)

## CONTENTS

I.	Introduction	2
II.	Formulation of the compositeness-relation and decay-width method	5
III.	Flatté parameterization and the spectral density of a bare state	10
	A. Spectral density and its integration	16
	B. Reinterpretation of the method of Sec. II for poles in the Riemann sheet II	16
IV.	Results and discussions using the total compositeness as input	18
	A. The $f_0(980)$ resonance	18
	B. The $a_0(980)$ resonance	21
V.	Results and discussions using the branching ratio $r_{\text{exp}}$ as input	23
	A. The $f_0(980)$ resonance	24
	B. The $a_0(980)$ resonance	32
VI.	Summary and conclusions	36
	Acknowledgments	37
	References	37

## I. INTRODUCTION

The non-perturbative meson–meson interactions and the related scalar-meson spectroscopy is a topic of great importance. The nature of scalar mesons is still under debate, in spite of the efforts during several decades in the past, particularly since the discovery of the resonances  $f_0(980)$  [1] and  $a_0(980)$  [2]. The scalar mesons below 1 GeV, like the  $f_0(500)/\sigma$ ,  $K^*(800)/\kappa$ ,  $f_0(980)$ ,  $a_0(980)$ , are serious candidates to comprise a  $J^{PC} = 0^{++}$  nonet as required in Refs. [3–9]. These resonances with vacuum quantum numbers are crucial for the deep understanding of spontaneous chiral symmetry breaking of Quantum Chromodynamics (QCD), its spectroscopy and, in general, of its non-perturbative nature [10–15]. Along the decades the lightest scalar resonances have been accommodated within different models like tetraquark states [3, 4, 16–19], molecular states [20–24], dynamically generated resonances [25–30], unitarized quark models [5, 31, 32], linear sigma models [33–36], etc.

For example, in Ref. [37] the  $a_0(980)$  is understood as a Breit-Wigner resonance, not as a dynamically generated resonance, while the  $f_0(980)$  is considered as a  $K\bar{K}$  bound state. We also notice that in Ref. [38] the compositeness is analyzed via the  $f_0(980) - a_0(980)$  mixing intensity, and it is found that the  $f_0(980)$  and  $a_0(980)$  cannot be simultaneously  $K\bar{K}$  bound states. The masses of the two resonances are very close and the  $f_0(980) - a_0(980)$  mixing could occur via the hadronic  $K\bar{K}$  loop [39–42]. Recently, there is also interest in assessing the nature of the scalar mesons by studying semileptonic decays [43–45]. For some reviews, see Refs. [46–49].

In fact, a meson has typically several components [50], such as the superposition of  $q\bar{q}$  and tetraquarks  $qq\bar{q}\bar{q}$  [51], gluonium [52], meson-meson components, etc. The compositeness, usually denoted by  $X$ , refers to the weight in the resonance state composition of the meson-meson components in the continuum part of the free spectrum [53, 54]. Therefore, it is a fundamental concept that is required for a quantitative analysis on the nature of the resonance. In contrast, the elementariness, typically called  $Z$ , is the weight of the bare (compact/short-range) degrees of freedom in the resonance constitution such that  $1 = Z + X$ .

For a bound state case, the compositeness is a positive real number [53] between 0 and 1 (as it should be), but its straightforward extension to the resonance case gives rise to complex-valued results [54]. Several extensions have been proposed [55–60] to end with real sensible values for the compositeness. In this work, we use the results of Refs. [54, 61] that allow a probabilistic interpretation of the compositeness relation of the resonance into open channels. Studies along these lines have also been extensively done for the case of heavy-quark resonances [62–68]. In addition, we also employ the formalism based on the evaluation of the spectral density function of the bare state associated to the resonance [69] by using a Flatté parameterization [55]. We then compare between this formalism and the one previously referred for the evaluation of the compositeness and elementariness, finding compatible results between them.

The  $f_0(980)$  and  $a_0(980)$  resonances couple mainly to the channels  $\pi\pi-K\bar{K}$  and  $\pi\eta-K\bar{K}$ , respectively. The main equations stem from considering the saturation of the compositeness relationship and the total width of the resonance, from which we calculate the couplings, partial compositeness coefficients and partial-decay widths. The implication of the branching ratio to the lighter channel, which we call  $r_{\text{exp}}$ , together with the reproduction of the total width, is also explored within our compositeness formalism. This set up allows to obtain more definite predictions for  $X$ , and the smaller the branching ratio the larger the resulting  $X$  by a linear relation. In particular, for the  $f_0(980)$  the branching ratio  $r_{\text{exp}} = 0.52 \pm 0.12$  [70], the most recent one collected in the PDG [49] from  $B$  decays to  $K\pi\pi$ , implies the largest  $X$  ranging around 0.6–0.9 within errors. In turn for the  $a_0(980)$  the branching ratios reported recently [49, 71] are much larger and then  $X$  calculated here

is significantly smaller, around  $0.2 - 0.4$ , taking into account errors and variations in the method of calculation. This indicates that other components in addition to the meson-meson ones play an important role in the constitution of the  $a_0(980)$ . However, it is worth keeping in mind that the most sophisticated theoretical studies on  $\pi\eta$  scattering matched with lattice QCD [72, 73] obtain that the  $a_0(980)$  is a pole lying in a hidden Riemann sheet from the physical energy axis. This was also obtained before in Refs. [74, 75]. At this point there is a caveat, because our study here cannot be applied to such scenario (in which the resonance effects manifest as a strong cusp) in order to clarify the nature of the  $a_0(980)$ . We find that for the  $f_0(980)$  the  $K\bar{K}$  component has a much larger partial compositeness coefficient than the  $\pi\pi$  channel. For the  $a_0(980)$  it is obtained that still the  $K\bar{K}$  compositeness coefficient is also larger than the one of the  $\pi\eta$ , but not overwhelmingly dominant. These results are a verification of those already obtained in Refs. [25, 29], such that if the  $\pi\eta$  channel were removed the  $a_0(980)$  would disappear, while the  $f_0(980)$  would keep appearing as a  $K\bar{K}$  bound state.

In connection with our use of Flatté parameterization we stress the importance of distinguishing between bare and renormalized couplings and widths. The former ones are those appearing directly in the Flatté parameterization, while the latter ones are associated to the actual residues of the partial-wave amplitude of interest at the pole position in the complex energy plane. We also show that for the present two-channel coupled scattering, when the pole lies in the second Riemann sheet, one has to modify the interpretation of the theoretically calculated partial-decay width to the lighter channel in terms of renormalized couplings (residues), and give the proper interpretation. These two effects explain why bare partial-decay widths, often found in the literature, are much bigger than those actually measured.

For the rest of the paper, Sec. II is dedicated to elaborate the formalism based on the saturation of the total compositeness and decay width of the resonance. In turn, Sec. III develops the method based on the use of a Flatté parameterization and introduces the spectral density function for a near-threshold resonance. Then, we apply these methods to the study of the  $f_0(980)$  and  $a_0(980)$  resonances, either by taking  $X$  as input in Sec. IV, or by using  $r_{\text{exp}}$  in Sec. V. In terms of them we typically provide the resulting partial compositeness coefficients and partial-decay widths. Finally, concluding remarks are given in Sec. VI.

## II. FORMULATION OF THE COMPOSITENESS-RELATION AND DECAY-WIDTH METHOD

For definiteness, we proceed with the discussion on the components in the nature of the  $f_0(980)$ , and develop a method to investigate its partial-decay widths, couplings and compositeness. Later on we also apply this method to the related isovector scalar resonance  $a_0(980)$ .

In what follows, we consider two main decay channels ( $\pi\pi$  and  $K\bar{K}$ ) of the  $f_0(980)$ . We follow the standard convention such that compositeness and elementariness coefficients are written as  $X$  and  $Z$ , respectively, with  $X + Z = 1$ . For the case of a bound state the coefficient  $Z$  corresponds to the field renormalization constant [53, 76], being real and positive and less than 1 (as  $X$  is too). The straightforward generalization for resonances of the compositeness and elementariness gives rise to complex numbers. As mentioned in the Introduction, several variants for the compositeness of a resonance have been discussed in the literature. Here we will follow Ref. [61], which formulates a probabilistic interpretation of the compositeness relation involving only positive and real coefficients for the resonance. As explained in Ref. [54] the compositeness  $X$  arises by evaluating the expected value of the number of mesons in the resonance divided by 2 (because we are considering two-body meson states). After the proper unitary phase transformation of the  $S$ -matrix, it gives the partial compositeness coefficient for the resonance in the form [61]

$$X_i = \left| \gamma_i^2 \right| \left| \frac{\partial G_i(s)}{\partial s} \right|_{s=s_R}, \quad (1)$$

and the subscript  $i$ , with  $i = 1$  and  $2$ , corresponds to the  $S$ -wave isoscalar  $\pi\pi$  and  $K\bar{K}$  channels, respectively. The pole position in the Mandelstam variable  $s$  is called  $s_R$ ,

$$s_R = (m_R - \frac{i}{2}\Gamma_R)^2, \quad (2)$$

with  $m_R$  and  $\Gamma_R$  the mass and width of the resonance, respectively. Furthermore,  $\gamma_i$  is the coupling of the resonance to the channel  $i$  that is extracted from the residues of the  $T$  matrix at the pole position  $s_R$ ,

$$\gamma_i^2 = - \lim_{s \rightarrow s_R} (s - s_R) T(s)_{ii}. \quad (3)$$

$G_i(s)$  is the unitary two-point scalar loop function for the  $i$ th channel and it can be written in the form [74]

$$G_i(s) = \frac{1}{16\pi^2} \left\{ a_i(\mu) + \log \frac{m_2^2}{\mu^2} - \frac{\Delta + s}{s} \log \frac{m_2}{m_1} + \frac{p_i}{\sqrt{s}} [\log(s - \Delta + 2\sqrt{s}p_i) + \log(s + \Delta + 2\sqrt{s}p_i) - \log(-s + \Delta + 2\sqrt{s}p_i) - \log(-s - \Delta + 2\sqrt{s}p_i)] \right\}. \quad (4)$$

Here  $\Delta = m_1^2 - m_2^2$  and  $m_1, m_2$  are the masses of the two particles in the channel  $i$ . We do not take into account the isospin breaking effects and use an average mass of the charged and neutral

pions, and proceed analogously for kaons too. However, such effects are expected to be negligible in our exploration. The term  $a_i(\mu) + \log \frac{m_2^2}{\mu^2}$  in Eq. (4) is independent of  $s$  and it disappears when taking the derivative of  $G_i(s)$  in Eq. (1). Finally in Eq. (4),  $p_i$  is the momentum of the channel  $i$ ,

$$p_i(s) = \frac{\sqrt{[s - (m_1 + m_2)^2][s - (m_1 - m_2)^2]}}{2\sqrt{s}} \quad (5)$$

The total compositeness coefficient,  $X = \sum_{i=1}^n X_i$ , is the sum over the partial compositeness coefficients  $X_i$ , and it must satisfy the condition  $X \leq 1$ . As discussed in more detail in Ref. [61], Eq. (1) is properly applied to the calculation of  $X_i$  for the channel  $i$  under the condition that the resonance lies in an unphysical Riemann sheet (RS) that is connected with the physical RS along an interval of the real- $s$  axis (where  $s$  is the total energy squared in the center of mass reference frame), lying above the threshold for the channel  $i$ .

Eq. (1) is very similar to that for a bound state case, see e.g. [54],

$$X_i = -\gamma_i^2 \left. \frac{\partial G_i(s)}{\partial s} \right|_{s=s_R}, \quad (6)$$

with the difference concerning the introduction of the absolute values.

It is necessary to distinguish the RS in which  $s_R$  lies. For the different signs of the imaginary part of  $p_1$  and  $p_2$  in the complex- $s$  plane, we can define the four different RSs as

$$\begin{aligned} \text{Sheet I : } & \text{Imp}_1 > 0, \text{ Imp}_2 > 0 \\ \text{Sheet II : } & \text{Imp}_1 < 0, \text{ Imp}_2 > 0 \\ \text{Sheet III : } & \text{Imp}_1 < 0, \text{ Imp}_2 < 0 \\ \text{Sheet IV : } & \text{Imp}_1 > 0, \text{ Imp}_2 < 0 \end{aligned} \quad (7)$$

The RSs II and III are connected to the physical RS I from the  $\pi\pi$  threshold onwards up to and above the  $K\bar{K}$  threshold in the real- $s$  axis, respectively. The threshold of the  $\pi\pi$  channel is distant from the resonance mass, while the resonance location is remarkably close to the  $K\bar{K}$  threshold, cf. Eq. (9) below.

Next, let us discuss how to make the analytical extrapolation from the RS I to the RSs II, III, IV in order to calculate the partial compositeness coefficient  $X_i$ , attending to the RS in which the pole lies. We have to cross the cut of  $G_i(s)$  and use its continuity property for real values of  $s$  with  $s > (m_{i,1} + m_{i,2})^2$ , where  $m_{i,1}$  and  $m_{i,2}$  are the masses of the first and second particles in the  $i_{\text{th}}$  channel, respectively. Then, one has that [25]

$$\begin{aligned} G_i^{\text{II}}(s + i\epsilon) &= G_i^{\text{I}}(s - i\epsilon) = G_i^{\text{I}}(s + i\epsilon) - 2i\text{Im}G_i^{\text{I}}(s + i\epsilon) \\ &= G_i^{\text{I}}(s + i\epsilon) + \frac{i}{8\pi} \sqrt{\frac{[s + i\epsilon - (m_1 + m_2)^2][s + i\epsilon - (m_1 - m_2)^2]}{(s + i\epsilon)^2}}, \end{aligned} \quad (8)$$

where the square root is calculated in the first Riemann sheet, with the argument of the radicand between 0 and  $2\pi$ . The Eq. (8) can be extrapolated to any other complex value of  $s$ . Thus, the RS I is obtained with  $G_1^I(s), G_2^I(s)$ ; the RS II corresponds to take  $G_1^{II}(s), G_2^I(s)$ ; the RS III is obtained with  $G_1^{II}(s), G_2^{II}(s)$ ; and the RS IV implies  $G_1^I(s), G_2^{II}(s)$ .

The crucial inputs in the evaluation of the coefficients  $X_i$ , Eq. (1), are the pole position and the coupling  $|\gamma_i|$ . Regarding the pole parameters of the  $f_0(980)$ , we preferentially consider the results obtained by the dispersive analysis of Ref. [77] based on the use of a set of Roy-like equations called the GKPY equations [78]. The mass and width of the resonance calculated in Ref. [77] are

$$m_R = 996 \pm 7 \text{ MeV}, \quad \Gamma_R = 50_{-12}^{+20} \text{ MeV}, \quad (9)$$

which provides a rather accurate determination for the mass, while the width is affected by rather large errors. When using this pole we consider the RS II because it was found to be there in the original publication [77].

In addition we consider the  $f_0(980)$  pole position from Ref. [74]. This reference performs an exhaustive study of  $S$  and  $P$ -wave meson-meson scattering by unitarizing one-loop amplitudes in  $U(3) \otimes U(3)$  Chiral Perturbation Theory [79–85] with explicit exchange of resonances. A large amount of experimental data on different reactions is reproduced and, at the same time, the consistency of the approach is checked by properly reproducing QCD constraints from spectral sum rules and semilocal duality as a function of the number of colors of QCD. The resulting pole of the  $f_0(980)$ , found also in the RS II, is

$$m_R = 978_{-11}^{+7} \text{ MeV}, \quad \Gamma_R = 58_{-22}^{+18} \text{ MeV}. \quad (10)$$

Interestingly for this case the mass of the resonance lies clearly below the  $K\bar{K}$  threshold, while  $m_R$  from Ref. [77] in Eq. (9) is above. In this way we can now explore what is the effect of such a relative arrangement of the resonance mass with respect to the two-kaon threshold. Instead, the width of the  $f_0(980)$  is rather similar in both cases.

In our considerations, we ignore the multiparticle  $4\pi$  channel whose contributions are very small up to 1 GeV as obtained in phenomenological studies where it is considered [78, 86], or estimated theoretically in studies based on unitarizing Chiral Perturbation Theory [87]. We simply notice as well that the electromagnetically driven two-photon decay channel has been ignored in our calculations. References [23, 49, 88, 89] obtained that  $\Gamma_{f_0(980) \rightarrow \gamma\gamma} = 0.32 \pm 0.05 \text{ MeV}$ , which contributes a tiny portion of the total width for the  $f_0(980)$ , and should be much smaller than the one for  $\pi\pi$ , and  $K\bar{K}$ .

Then, we sensibly assume that the total compositeness coefficient of  $f_0(980)$  can be expressed

as the sum of the  $S$ -wave isoscalar  $\pi\pi$  and  $K\bar{K}$  channels,

$$X = X_1 + X_2 = |\gamma_1|^2 \left| \frac{\partial G_1(s)}{\partial s} \right|_{s=s_R} + |\gamma_2|^2 \left| \frac{\partial G_2(s)}{\partial s} \right|_{s=s_R}. \quad (11)$$

In addition to Eq. (11), another main equation stems from imposing the saturation of the width of the  $f_0(980)$ . As the threshold of the  $\pi\pi$  channel is distant from the resonance we use the standard formula for the partial-decay width of the  $f_0(980)$  to  $\pi\pi$ ,

$$\Gamma_1 = \frac{|\gamma_1|^2 p_1(m_R^2)}{8\pi m_R^2}, \quad (12)$$

where  $p_i$  is the momentum in the rest frame of the resonance, cf. (5) with  $s = m_R^2$ .

However, the  $K\bar{K}$  threshold is very close to the resonance mass and the effect of the finite width of the  $f_0(980)$  (around 50 MeV) in the  $K\bar{K}$  phase space is not negligible. Notice that even the lower limit of the  $f_0(980)$  mass within its uncertainty region in Eq. (9) is indeed smaller than the  $K\bar{K}$  threshold. However, since the uncertainty in the mass is much smaller than the width of the resonance, this fact is easily overturned by the mass distribution of the resonance and it does not prevent the actual decay of the  $f_0(980)$  to  $K\bar{K}$ , even when the resonance mass is below the  $K\bar{K}$  threshold.

In these regards, we consider a Lorentzian mass distribution for the resonance, and the partial-decay width is written as

$$\Gamma_2 = \frac{|\gamma_2|^2}{16\pi^2} \int_{m_1+m_2}^{+\infty} dW \frac{p_2(W^2)}{W^2} \frac{\Gamma_R}{(m_R - W)^2 + \Gamma_R^2/4} \quad (13)$$

In the limit  $\Gamma_R \rightarrow 0$ , Eq. (13) becomes the standard formula for the decay width. In a practical calculation, the upper limit of integration ( $+\infty$ ) is replaced by  $m_R + n\Gamma_R$ . For example, in Ref. [63], the value of  $n = 8$  is chosen for the  $Z_b(10610)/Z_b(10650)$  by reproducing the experimental width; in Ref. [66],  $n = 10$  is adopted for the  $Z_c(3900)$ ,  $X(4020)$  and  $Z_c(3985)$  particles. However, in the Ref. [62], dedicated to the study of the compositeness of the  $\chi_{c1}p$  for the  $P_c(4450)$ , the upper limit of integration used was  $m_R + 2\Gamma_R$ . The region for  $n = 2$  is usually thought to be a reasonable cut in the resonance region [62, 90]. For our consideration, we restrict the upper integration limit in the resonance region to  $m_R + 2\Gamma_R$  (which comprises the resonance signal as it can be seen in Fig. 2, introduced in Sec. III within the context of a Flatté parameterization).

Another aspect to take into account is the RS in which the pole lies because the sign of the momentum of the kaons in the center of mass reference frame has opposite signs in the RSs II and III at the pole position. Notice that for the latter RS the kaon momentum has the standard sign in the lower complex-energy half-plane, corresponding to a  $m_R - i\Gamma_1/2 - i\Gamma_2/2$ , while for the former one has instead  $m_R - i\Gamma_1/2 + i\Gamma_2/2$ . Because this change of sign in the kaon momentum the

saturation of the resonance width obtained from the pole position varies, such that  $\Gamma_2$  standardly adds to  $\Gamma_1$  when the pole lies in the RS III, but  $\Gamma_2$  *subtracts from*  $\Gamma_1$  when the pole lies in the RS II. As a result, the total decay width of the  $f_0(980)$  is then

$$\Gamma_R = |\gamma_1|^2 \frac{p_1(m_R^2)}{8\pi m_R^2} \pm \frac{|\gamma_2|^2}{16\pi^2} \int_{m_1+m_2}^{m_R+2\Gamma_R} dW \frac{p(W^2)}{W^2} \frac{\Gamma_R}{(m_R - W)^2 + \Gamma_R^2/4}, \quad (14)$$

for the pole in the RS III or II, respectively.

Another interesting consequence of this discussion on the RS in which the pole lies is the simple observation that for a pole in the RS II the combination  $m_R - i\Gamma_1/2 + i\Gamma_2/2$  can be rewritten as  $m_R - i(\Gamma_1 - 2\Gamma_2)/2 - i\Gamma_2/2$ , so that now the decay width to  $K\bar{K}$  appears with the right sign in the resonance propagator for an interpretation as a decay width, while the decay width to the lighter channel is  $\Gamma_1 - 2\Gamma_2$ . This result can also be obtained in a more straightforward mathematical way in terms of the branching ratio to the first channel,  $r_{\text{exp}}$ , by noticing that

$$r_{\text{exp}} = 1 - \frac{\Gamma_2}{\Gamma_R} = \frac{\Gamma_R - \Gamma_2}{\Gamma_R} = \frac{\Gamma_1 - 2\Gamma_2}{\Gamma_R}, \quad \text{RS II}, \quad (15)$$

where we have used again that  $\Gamma_R = \Gamma_1 - \Gamma_2$ . However, for a pole in the RS III one has the standard result

$$r_{\text{exp}} = 1 - \frac{\Gamma_2}{\Gamma_R} = \frac{\Gamma_1}{\Gamma_R}, \quad \text{RS III}. \quad (16)$$

Nonetheless, in what follows, we keep the usual notation of directly calling  $\Gamma_i$  as decay widths, though for  $i = 1$  and the pole in the RS II the actual decay width to the lighter channel does not coincide with  $\Gamma_1$ , as just discussed. Because of this reason we denote by  $\Gamma_{\pi\pi}$  or  $\Gamma(f_0(980) \rightarrow \pi\pi)$  the physical decay width of the  $f_0(980)$  to  $\pi\pi$ , and similarly we use  $\Gamma_{\pi\eta}$  or  $\Gamma(f_0(980) \rightarrow \pi\eta)$  for the physical partial-decay width of the  $a_0(980)$  to the lighter channel. For  $K\bar{K}$  we can use indistinctly  $\Gamma_2$  or  $\Gamma_{K\bar{K}}$  since they coincide. They have the same meaning as  $\Gamma(f_0(980) \rightarrow K\bar{K})$  or  $\Gamma(a_0(980) \rightarrow K\bar{K})$  in a clear notation.

These points are further elaborated when considering a Flatté parameterization for the  $f_0(980)$  and  $a_0(980)$  resonances in Sec. III.

Combining Eq. (11) and Eq. (14) allows us to solve  $|\gamma_1|$  and  $|\gamma_2|$  in terms of the total compositeness and width. Then we can obtain the partial-decay width  $\Gamma_i$  and individual compositeness coefficient  $X_i$  for each channel.<sup>1</sup> We consider several choices for  $X$  in Eq. (11), typically from 0.2 up to 0.8 in steps of 0.2.

<sup>1</sup> The fact that the width of the  $f_0(980)$  is substantially larger than the difference between its mass and the  $K\bar{K}$  threshold allows to apply in a reasonable way the standard formula Eq. (1) for the partial compositeness  $X_2$ , even if the  $f_0(980)$  pole lies in the 2nd (3rd) RS above (below) the *nearby*  $K\bar{K}$  threshold. The mass distribution of the resonance smooths the sharp condition, alluded after Eq. (5), on the relative position between the resonance mass and the threshold of  $K\bar{K}$  when their distance is much smaller than the  $f_0(980)$  width.

The information for the branching ratio  $r_{\text{exp}} = \Gamma(f_0(980) \rightarrow \pi\pi)/[\Gamma(f_0(980) \rightarrow \pi\pi) + \Gamma(f_0(980) \rightarrow K\bar{K})]$  can also be used together with the total width  $\Gamma_R$  to fix  $|\gamma_1|$  and  $|\gamma_2|$ . The results following one way or the other are organized in Secs. IV and V, respectively. They are also applied in analogous way to the isovector scalar  $a_0(980)$  involving the scattering channels  $\pi\eta(1)$  and  $K\bar{K}(2)$ , with  $r_{\text{exp}} = \Gamma(a_0(980) \rightarrow \pi\eta)/[\Gamma(a_0(980) \rightarrow \pi\eta) + \Gamma(a_0(980) \rightarrow K\bar{K})]$  then.

### III. FLATTÉ PARAMETERIZATION AND THE SPECTRAL DENSITY OF A BARE STATE

One disadvantage of the approach followed in Sec. II is the necessity to assume a value of  $n$  for the upper limit of integration in Eq. (13) for evaluating the partial-decay width of the resonance into  $K\bar{K}$ , that is,  $\Gamma_2$ . This can be overcome by using a Flatté parameterization [91], without increasing the number of the input parameters needed to calculate the couplings  $|\gamma_i|$ , partial-decay widths  $\Gamma_i$  and partial compositeness coefficients  $X_i$ . Since the  $f_0(980)$  and  $a_0(980)$  lie very close to the  $K\bar{K}$  threshold a Flatté parameterization is then specially suitable [55]. Nonetheless, as discussed in Refs. [64, 92], there is also a limitation in the use of a Flatté parameterization as it assumes that the corresponding  $K\bar{K}$  partial-wave amplitude has no zero in the near-threshold region. We assume that this is the case and proceed with the rather intuitive picture offered by a Flatté parameterization of dressing a bare resonance propagator,  $1/D(E)$ , by the self energy due to the intermediate channels 1 and 2,

$$D(E) = E - E_f + i\frac{\tilde{\Gamma}_1}{2} + \frac{i}{2}g_2\sqrt{m_K E}. \quad (17)$$

Here  $E$  is the total center of mass energy measured with respect to the two-kaon threshold,  $E \equiv \sqrt{s} - 2m_K$ ,  $E_f$  is the bare mass of the resonance plus the contributions at around the  $K\bar{K}$  threshold from the real parts (which are taken as constants) of the meson-meson loops contributing to the resonance self energy. In addition,  $g_i$  is the *bare* coupling squared of the resonance to the  $i_{\text{th}}$  channel, such that the *bare* width  $\tilde{\Gamma}_1$  to channel 1 is written in terms of  $g_1$  as

$$\tilde{\Gamma}_1 = \frac{p_1(m_R)g_1}{8\pi m_R^2}. \quad (18)$$

The pole position in the variable  $E$  is called  $E_R = M_R - i\Gamma_R/2$ , with  $M_R$  the mass of the resonance with respect to  $2m_K$ ,  $M_R = m_R - 2m_K$ .

The Flatté parameterization contains as free parameters  $E_f$ ,  $\tilde{\Gamma}_1$  and  $g_2$  that can be fixed in terms of the mass and width of the resonance, that is, by knowing its pole position, and from the knowledge either of the branching ratio  $r_{\text{exp}}$  to the lighter channel or the total compositeness  $X$ .

To calculate the resonance pole position we must look for the zeroes of Eq. (17),  $D(E_R) = 0$ ,

$$E_R - E_f + \frac{i}{2} \tilde{\Gamma}_1 = -\frac{i}{2} g_2 \sqrt{m_K E_R}. \quad (19)$$

Taking the square in both sides of the previous expression and solving the resulting quadratic algebraic equation, we then have the following solutions for the roots

$$E_R = E_f - \frac{1}{8} m_K g_2^2 - \frac{i}{2} \tilde{\Gamma}_1 + \sigma \sqrt{\frac{m_K g_2^2}{4}} \sqrt{\frac{m_K g_2^2}{16} - E_f + \frac{i}{2} \tilde{\Gamma}_1}, \quad (20)$$

with  $\sigma = \pm 1$  in order to keep track of the two different solutions. Later on we show that  $\sigma = +1(-1)$  corresponds to the pole lying in the RS II (III). For the calculation of the square root in the previous equation (taken such that  $\Im\sqrt{z} \geq 0$ ,  $z \in \mathbb{C}$ ) one needs to distinguish two cases according to the sign of  $m_K g_2^2/16 - E_f$ :

$$\text{i) } \frac{m_K g_2^2}{16} - E_f > 0, \quad (21)$$

$$E_R = E_f - \frac{i}{2} \tilde{\Gamma}_1 - \frac{m_K g_2^2}{8} + \frac{\sigma}{2} \sqrt{m_K g_2^2} \left( \left( \frac{m_K g_2^2}{16} - E_f \right)^2 + \frac{\tilde{\Gamma}_1^2}{4} \right)^{\frac{1}{4}} \exp \left( -\frac{i}{2} \arctan \frac{\tilde{\Gamma}_1/2}{E_f - m_K g_2^2/16} \right).$$

$$\text{ii) } \frac{m_K g_2^2}{16} - E_f < 0, \quad (22)$$

$$E_R = E_f - \frac{i}{2} \tilde{\Gamma}_1 - \frac{m_K g_2^2}{8} + \frac{\sigma}{2} \sqrt{m_K g_2^2} \left( \left( \frac{m_K g_2^2}{16} - E_f \right)^2 + \frac{\tilde{\Gamma}_1^2}{4} \right)^{\frac{1}{4}} \exp \frac{i}{2} \left( \pi - \arctan \frac{\tilde{\Gamma}_1/2}{E_f - m_K g_2^2/16} \right).$$

In what follows we only consider the case i), because for both i) and ii) one obtains the same equations relating  $E_f$ ,  $g_2$  and  $\tilde{\Gamma}_1$  with the inputs  $M_R$ ,  $\Gamma_R$  and  $r_{\text{exp}}$  or  $X$ . We introduce the auxiliary angle  $\phi$  defined by

$$\phi = \arctan \frac{\tilde{\Gamma}_1/2}{E_f - m_K g_2^2/16}. \quad (23)$$

Therefore,  $E_R$  can be written as

$$E_R = E_f - \frac{m_K g_2^2}{8} - \frac{i}{2} \tilde{\Gamma}_1 + \frac{\sigma}{2} \sqrt{m_K g_2^2} \left( \left( E_f - \frac{m_K g_2^2}{16} \right)^2 + \frac{\tilde{\Gamma}_1^2}{4} \right)^{\frac{1}{4}} \left( \cos \frac{\phi}{2} - i \sin \frac{\phi}{2} \right). \quad (24)$$

Attending to the real and imaginary parts in this equation we have that

$$M_R = E_f - \frac{m_K g_2^2}{8} + \sigma \frac{\sqrt{m_K g_2^2}}{2} \left( \left( E_f - \frac{m_K g_2^2}{16} \right)^2 + \frac{\tilde{\Gamma}_1^2}{4} \right)^{\frac{1}{4}} \cos \frac{\phi}{2}, \quad (25)$$

$$\Gamma_R = \tilde{\Gamma}_1 + \sigma \sqrt{m_K g_2^2} \left( \left( E_f - \frac{m_K g_2^2}{16} \right)^2 + \frac{\tilde{\Gamma}_1^2}{4} \right)^{\frac{1}{4}} \sin \frac{\phi}{2}.$$

Taking into account the definition of  $\phi$ , one also has that

$$\left(E_f - \frac{m_K g_2^2}{16}\right)^2 + \frac{\tilde{\Gamma}_1^2}{4} = \left(E_f - \frac{m_K g_2^2}{16}\right)^2 (1 + \tan^2 \phi) = \left(E_f - \frac{m_K g_2^2}{16}\right)^2 \frac{1}{\cos^2 \phi}, \quad (26)$$

and

$$E_f - \frac{m_K g_2^2}{16} = \frac{\tilde{\Gamma}_1}{2} \cot \phi. \quad (27)$$

Substituting these two equalities into Eq. (25), with  $\phi < 0$  for case i), the latter equation becomes

$$\begin{aligned} M_R &= -\frac{m_K g_2^2}{16} + \frac{\tilde{\Gamma}_1}{2} \cot \phi + \frac{\sigma}{4} \sqrt{m_K g_2^2 \tilde{\Gamma}_1 |\cot \frac{\phi}{2}|}, \\ \Gamma_R &= \tilde{\Gamma}_1 - \frac{\sigma}{2} \sqrt{m_K g_2^2 \tilde{\Gamma}_1 |\tan \frac{\phi}{2}|}. \end{aligned} \quad (28)$$

From this last equation it follows that

$$\frac{\sigma}{2} \sqrt{m_K g_2^2 \tilde{\Gamma}_1} = (\tilde{\Gamma}_1 - \Gamma_R) \sqrt{|\cot \frac{\phi}{2}|}. \quad (29)$$

When this is taken into Eq. (28) we can write  $M_R$  as

$$\begin{aligned} M_R &= \frac{\Gamma_R^2}{4\tilde{\Gamma}_1} \cot \frac{\phi}{2} \left[ 1 - \left( \frac{\tilde{\Gamma}_1}{\Gamma_R} \tan \frac{\phi}{2} \right)^2 \right], \\ \Gamma_R &= \tilde{\Gamma}_1 - \frac{\sigma}{2} \sqrt{m_K g_2^2 \tilde{\Gamma}_1 |\tan \frac{\phi}{2}|}. \end{aligned} \quad (30)$$

The equation for  $M_R$  is of the form,

$$\begin{aligned} x - \frac{1}{x} &= \frac{4M_R}{\Gamma_R}, \\ x &\equiv \frac{\Gamma_R}{\tilde{\Gamma}_1} \cot \frac{\phi}{2} < 0, \end{aligned} \quad (31)$$

and its solution for  $x < 0$  is

$$x = \frac{2M_R}{\Gamma_R} - \sqrt{1 + \left(\frac{2M_R}{\Gamma_R}\right)^2}. \quad (32)$$

After this is substituted in the expression for  $\Gamma_R$  in Eq. (30), we can isolate the bare partial-decay width to the first channel, and then the bare branching ratio  $r \equiv \tilde{\Gamma}_1/\Gamma_R$  is given by

$$\begin{aligned} r &= 1 + \frac{\sigma g_2 \sqrt{m_K}/2}{u - 2M_R}, \\ u &\equiv (4M_R^2 + \Gamma_R^2)^{1/2}. \end{aligned} \quad (33)$$

Once we know  $r$  we can also determine  $\cot \phi/2$  by using the definition of  $x$  and its solution in Eq. (32),

$$\cot \frac{\phi}{2} = rx = \frac{1}{2\Gamma_R} \left( 4M_R - 2u - \sigma g_2 \sqrt{m_K(u - 2M_R)} \right). \quad (34)$$

Let us denote by  $\beta$  the residue of  $1/D(E)$  at the resonance pole,

$$\beta = \left| \lim_{E \rightarrow E_R} \frac{E - E_R}{D(E)} \right| = \left| \frac{1}{1 + \frac{ig_2}{4} \sqrt{\frac{m_K}{E_R}}} \right| = \frac{\sqrt{8u}}{\left( g_2^2 m_K + 8u + 4\sigma g_2 \sqrt{m_K(u - 2M_R)} \right)^{1/2}}. \quad (35)$$

This expression can be obtained by substituting  $\sqrt{E_R}$  from Eq. (19), the relation between  $E_f$  and  $\tan \phi$ , cf. Eq. (27), and finally the expression for  $\tan \phi$  from that of  $\cot \phi/2$  given in Eq. (34).

The *renormalized or dressed* coupling squared  $|\gamma_i^2|$  is related to the bare one  $g_i$  by evaluating the residue of the elastic scattering amplitudes for channel  $i$ ,  $g_i/D(E)$ . In terms of  $\beta$ , we have the result

$$\begin{aligned} |\gamma_1|^2 &= g_1 \beta, \\ |\gamma_2|^2 &= 32\pi m_K^2 g_2 \beta, \end{aligned} \quad (36)$$

with the numerical factor in front of  $g_2\beta$  needed for having the same normalization as in Sec. II.

Up to our knowledge the difference between the bare and dressed couplings in a Flatté parameterization has not been clearly discussed before in the literature, and it has important implications. E.g. this is one of the reasons why the values for  $\tilde{\Gamma}_{\pi\pi}$  collected in the Table 2 of Ref. [55] for the  $f_0(980)$  are typically much bigger than 100 MeV. A similar comment can also be made for most of the entries of  $\tilde{\Gamma}_{\pi\eta}$  in Table 1 of the same reference regarding the  $a_0(980)$ .<sup>2</sup> Indeed, this can be a source for confusion in the literature. In this respect, we notice that Ref. [77] compares their  $\pi\pi$   $S$ -wave residue with bare couplings used in energy-dependent-width Breit-Wigner or Flatté parameterizations without considering the actual residue at the resonance pole position of the parameterization.

In order to obtain  $g_2$  we need another input, for which we take either the physical branching ratio  $r_{\text{exp}}$  or the total compositeness  $X$ . For the latter case we need then the expression for calculating  $X_1$  and  $X_2$ , with  $X = X_1 + X_2$ . Recalling Eq. (1) we have for  $X_1$ ,

$$X_1 = \gamma_1^2 \left| \frac{\partial G_1}{\partial s} \right|_{s=s_R} = \frac{8\pi m_R^2 \Gamma_R}{p_1(m_R)} r \beta \left| \frac{\partial G_1}{\partial s} \right|_{s=s_R}, \quad (37)$$

<sup>2</sup> The other reason applies to those poles in the RS II because then the physical partial-decay width to the lighter channel is  $\Gamma_1 - 2\Gamma_2$ , which is smaller than  $\Gamma_1$ , cf. Eq. (15) and discussions below in this section.

with  $r$  and  $\beta$  given in terms of  $g_2$  and the pole parameters in Eqs. (33) and (35), respectively. For the calculation of  $X_2$  a simpler algebraic formula can be obtained if we use non-relativistic kinematics for the calculation of the derivative of  $\partial G_2(s)/\partial s$  at  $s = s_R$ , taking advantage of the fact that pole lies in the vicinity of the  $K\bar{K}$  threshold. Then,  $G_2(s)$  is a constant plus  $-i\sqrt{m_K E}/(16\pi m_K) + \mathcal{O}(E/m_K)$ , and its derivative with respect to  $s$  is

$$\left. \frac{\partial G_2(s)}{\partial s} \right|_{s_R} = \frac{-i}{128\pi m_K^{3/2} \sqrt{E_R}} + \mathcal{O}(1). \quad (38)$$

We then multiply this derivative by  $32\pi m_K^2 g_2 \beta$  and the final expression that results is

$$X_2 = \frac{\sqrt{m_K} g_2}{\left( g_2^2 m_K + 8u + 4\sigma g_2 \sqrt{m_K} (u - 2M_R) \right)^{\frac{1}{2}}}. \quad (39)$$

The equation that is needed to be solved to obtain  $g_2$  given  $X$  is  $X_1 + X_2 = X$ . Nonetheless, in the numerical results shown below we calculate  $X_2$  making use of relativistic kinematics, with differences of around a 10–15% compared with the values obtained when using the non-relativistic Eq. (39).

When  $r_{\text{exp}}$  is the input taken one has to distinguish between whether the pole lies in the RS II or RS III, due to the change of sign in the analytical extrapolation of  $\sqrt{E}$  in  $D(E)$ , Eq. (17), needed to reach the pole position. For the pole in the RS III, we have the following straightforward relation between the physical  $r_{\text{exp}}$  and the bare  $r$ ,

$$r_{\text{exp}} = r\beta = \frac{\sqrt{2u} (2\sqrt{u - 2M_R} + g_2 \sigma \sqrt{m_K})}{\sqrt{u - 2M_R} \left( g_2^2 m_K + 8u + 4\sigma g_2 \sqrt{m_K} (u - 2M_R) \right)^{1/2}}. \quad (40)$$

This is a quadratic equation for  $g_2$  that can be easily solved. By requiring that  $g_2 = 0$  for  $r_{\text{exp}} = 1$  (which implies that there is no resonance decay at all to the  $K\bar{K}$  channel) then there is only one acceptable solution given by

$$g_2 = \frac{2 \left( -\Gamma_R r_{\text{exp}} + \sqrt{u - 2M_R} \sqrt{2M_R r_{\text{exp}}^2 + (2 - r_{\text{exp}}^2)u} \right)}{\sqrt{m_K} \left( 2M_R r_{\text{exp}}^2 + (2 - r_{\text{exp}}^2)u \right)}. \quad (41)$$

For a pole in the RS II, when moving to the complex- $E$  plane with negative imaginary part the square root  ${}^{\text{II}}\sqrt{E}$  has a positive imaginary part and negative real one, changing sign with respect to that when calculated in the RS III, because there  ${}^{\text{III}}\sqrt{E} = -{}^{\text{II}}\sqrt{E}$  (the momentum  $p_2$  changes sign between the two sheets). As a result, it is indeed the case that the last term in Eq. (17), responsible for the width to  $K\bar{K}$ , does not add to but subtract from  $\tilde{\Gamma}_1$ . Then, for a physical interpretation of the different terms in this equation it is convenient to rewrite it as

$$\begin{aligned} D(E) &= E - E_f + \frac{i}{2} \left[ \tilde{\Gamma}_1 + 2g_2 {}^{\text{II}}\sqrt{m_K E} \right] - \frac{i}{2} g_2 {}^{\text{II}}\sqrt{m_K E} \\ &= E - E_f + \frac{i}{2} \left[ \tilde{\Gamma}_1 - 2g_2 {}^{\text{III}}\sqrt{m_K E} \right] + \frac{i}{2} g_2 {}^{\text{III}}\sqrt{m_K E}. \end{aligned} \quad (42)$$

Let us notice that the real part of  $\sqrt[3]{M_R - i\Gamma_R/2}$  is positive and then the imaginary part of the last term in Eq. (42) appears with the same sign as  $\tilde{\Gamma}_1$ . From this equation we then deduce that, once the bare couplings are dressed, cf. Eq. (36), the partial-decay width to the lighter channel really observed in an experiment is not  $\Gamma_1$  but  $\Gamma_1 - 2\Gamma_2$ , while the total decay width  $\Gamma_R$  is  $\Gamma_1 - \Gamma_2$  for the RS II case. Therefore, when taking  $r_{\text{exp}}$  as input for a pole in the RS II,

$$r_{\text{exp}} = \frac{\Gamma_1}{\Gamma_R} - 2\frac{\Gamma_2}{\Gamma_R} = r\beta - 2(1 - r_{\text{exp}}) \quad (43)$$

from where the extra equation to be taken into account is:

$$2 - r_{\text{exp}} = r\beta = \frac{\sqrt{2u} (2\sqrt{u - 2M_R} + g_2\sigma\sqrt{m_K})}{\sqrt{u - 2M_R} \left( g_2^2 m_K + 8u + 4\sigma g_2 \sqrt{m_K(u - 2M_R)} \right)^{1/2}}, \quad (44)$$

instead of the straight Eq. (40) for a pole in the RS III. The valid solution in this case, the one that gives  $g_2 = 0$  for  $r_{\text{exp}} = 1$ , is obtained from Eq. (41) by simultaneously multiplying its right-hand side by a minus sign and replacing  $r_{\text{exp}}$  for  $2 - r_{\text{exp}}$ .

As a result of this analysis we then expect that  $\Gamma_1 > \Gamma_R$  with values in the interval  $[\Gamma_R, 2\Gamma_R]$  for the resonance when its pole lies in the RS II. To illustrate this point, let us take the residues given in the Refs. [74, 77] for the pole positions of the  $f_0(980)$  in Eqs. (9) and (10), respectively, and evaluate  $\Gamma_1/\Gamma_R$  making use of Eq. (12). The values of the residues are  $|\gamma_1| = 2.3 \pm 0.2$  GeV [77] and  $|\gamma_1| = 1.80 \pm 0.25$  GeV [74]. Propagating the errors in  $m_R$ ,  $\Gamma_R$  and  $|\gamma_1|$  from these references, the values that we obtain are

$$\begin{aligned} \frac{\Gamma_1}{\Gamma_R} &= 2.0 \pm 0.9, \text{ Eq. (9)–Ref. [77]}, \\ \frac{\Gamma_1}{\Gamma_R} &= 1.1 \pm 0.6, \text{ Eq. (10)–Ref. [74]}. \end{aligned} \quad (45)$$

This more detailed discussion based on the use of the Flatté parameterization extends the same topic already discussed in Sec. II for the interpretation of the  $\Gamma_i$ 's and their connection with the experimental decay widths for the case of a pole lying in the RS II.

It is worth stressing that when  $X$  is taken as input the procedure explained above, Eqs. (37)–(39), allows to calculate  $\Gamma_1/\Gamma_R$  without relying on its connection to  $r_{\text{exp}}$ , and the resulting values, which we discuss below, are perfectly compatible with the picture just explained.

Finally, let us now show the relationship between the sign  $\sigma$  and the RS in which the pole lies. For that, we isolate  $\sqrt{E_R}$  from Eq. (19), which can then be written as

$$\sqrt{E_R} = \frac{2i}{g_2\sqrt{m_K}}(M_R - E_f) + \frac{\Gamma_R - \tilde{\Gamma}_1}{g_2\sqrt{m_K}}. \quad (46)$$

This equation tells us that if  $M_R - E_f > 0$  the pole lies in the RS II, since then  $\Im\sqrt{E_R} > 0$  and, conversely, if  $M_R - E_f < 0$  the pole is located in the RS III. Now, we consider Eq. (25) which clearly implies that if  $\sigma = -1$  then  $M_R - E_f < 0$ , corresponding to the RS III. For  $\sigma = +1$  a more careful treatment is needed because the sign of  $M_R - E_f$  depends on the relative sign between the last two terms in the right-hand side of Eq. (25). One can straightforwardly show that the absolute value of the last term is bigger than  $m_K g_2^2/8$  by squaring and subtracting them. In the process one has to relate  $E_f$  with  $\tan \phi$ , Eq. (27), and use the expression for  $\cot \phi/2$  given in Eq. (34). As a result  $M_R - E_f > 0$  and the pole lies in the RS II for  $\sigma = +1$ .

We give the results obtained with the present formalism based on the use of the Flatté parameterization, distinguishing between when  $X$  or  $r_{\text{exp}}$  are taken as inputs in Secs. IV and V, respectively.

### A. Spectral density and its integration

Here we use the spectral density function  $\omega(E)$  of a near-threshold resonance, in our case either  $f_0(980)$  or  $a_0(980)$ , as a way to calculate the compositeness of the meson-meson states in these resonances. We follow the formalism of Ref. [55] to which we refer for further details. There the spectral density function  $\omega(E)$  is introduced, and it provides the probability distribution function in energy for finding a bare elementary state in the continuum [69]. As a result, its integration around the  $K\bar{K}$  threshold comprising the resonance signal, which we call  $W_R$ , is the probability for finding the bare state. Namely,  $W_R$  is calculated as [55]

$$W_R = \int_{-\Delta}^{+\Delta} dE \omega(E) , \quad (47)$$

$$\omega(E) = \frac{1}{2\pi} \frac{\tilde{\Gamma}_1 + g_2 \sqrt{m_K E} \theta(E)}{\left(E - E_f - \frac{1}{2} g_2 \sqrt{-m_K E} \theta(-E)\right)^2 + \frac{1}{4} \left(\tilde{\Gamma}_1 + g_2 \sqrt{m_K E} \theta(E)\right)^2} ,$$

with  $\theta(E)$  the Heaviside step function. In Ref. [55] the parameter  $\Delta$  was chosen to be 50 MeV but, since an important dependence on  $\Delta$  is observed on the final value of  $W_R$ , we prefer to present the results for  $W_R$  as a function of  $\Delta$ .

### B. Reinterpretation of the method of Sec. II for poles in the Riemann sheet II

By the application of the Flatté parameterization it has been clear that for a near-threshold pole in coupled channels lying in the RS II it is necessary to change the interpretation of  $\Gamma_1$ . We have seen from the last line in Eq. (42) that the partial-decay width into the lighter channel is

not directly  $\Gamma_1$  but  $\Gamma_1 - 2\Gamma_2$ , and that the total width from the pole position should be compared with  $\Gamma_1 - \Gamma_2$ .

Therefore, for a pole in the RS II near the heavier threshold the equation for the saturation of the total width, cf. Eq. (14), reads

$$\Gamma_R = |\gamma_1|^2 \frac{p_1(m_R^2)}{8\pi m_R^2} - \frac{|\gamma_2|^2}{16\pi^2} \int_{m_1+m_2}^{m_R+2\Gamma_R} dW \frac{p(W^2)}{W^2} \frac{\Gamma_R}{(m_R - W)^2 + \Gamma_R^2/4}, \quad (48)$$

with no change in Eq. (11) for saturating the total compositeness  $X$ . The latter equation is also reproduced here

$$X = |\gamma_1|^2 \left| \frac{\partial G_1(s)}{\partial s} \right|_{s=s_R} + |\gamma_2|^2 \left| \frac{\partial G_2(s)}{\partial s} \right|_{s=s_R}. \quad (49)$$

However, in applications up to now of these ideas instead of the minus in Eq. (48) a “standard” plus sign is placed in front of  $|\gamma_2|^2$ . Namely,

$$\Gamma_R = |\gamma_1|^2 \frac{p_1(m_R^2)}{8\pi m_R^2} + \frac{|\gamma_2|^2}{16\pi^2} \int_{m_1+m_2}^{m_R+2\Gamma_R} dW \frac{p(W^2)}{W^2} \frac{\Gamma_R}{(m_R - W)^2 + \Gamma_R^2/4}, \quad (50)$$

At the practical level as long as  $X_1 \ll X_2$  the only change is in the value of  $|\gamma_1|$ , because the use of Eq. (50) would provide an “effective” value of this coupling by reabsorbing the effect of subtracting  $-2\Gamma_2$  in Eq. (48). This is clear because then  $X$  is saturated almost completely by  $X_2$  and this quantity alone fixes  $|\gamma_2|$ . The use of Eq. (48) allows to determine  $|\gamma_1|$ , which is certainly larger than the “effective” one deduced by fulfilling Eq. (50) with an intermediate plus sign. However, the values for  $X_2$ ,  $\Gamma_2$  and the physical partial-decay width to channel 1 almost do not change, which are typically the most important pieces of information to infer about the nature of the resonances.

Now, if  $r_{\text{exp}}$  is taken as input the equations that one has to fulfill are Eq. (48) and

$$2 - r_{\text{exp}} = |\gamma_1|^2 \frac{p_1(m_R^2)}{8\pi m_R^2 \Gamma_R}, \quad (51)$$

which are apparently very different to the “standard” Eq. (50) and

$$r_{\text{exp}} = \frac{\Gamma_1}{\Gamma_R}, \quad (52)$$

already written for a pole in the RS III in Sec. II. However, they basically provide again the same results for  $\Gamma_2$ ,  $X_2$ , and the physical partial-decay width to channel 1, while the use of Eqs. (50) and (52) provides the already mentioned “effective” value for  $|\gamma_1|$ .

In order to see it, let us divide Eq. (48) by  $\Gamma_R$  and write the following equations equivalent to Eqs. (48) and (51),

$$1 = \frac{\Gamma_1}{\Gamma_R} - \frac{\Gamma_2}{\Gamma_R}, \quad (53)$$

$$2 - r_{\text{exp}} = \frac{\Gamma_1}{\Gamma_R}.$$

Subtracting the first line from the second one we then have

$$1 - r_{\text{exp}} = \frac{\Gamma_2}{\Gamma_R}, \quad (54)$$

which fixes  $|\gamma_2|$  as if Eq. (50) were used. Afterwards, Eq. (48) is employed to calculate  $|\gamma_1|$ , while the use of Eq. (50) would provide the so-called “effective” value for  $|\gamma_1|$ , which would be smaller than the one obtained from Eq. (48).

#### IV. RESULTS AND DISCUSSIONS USING THE TOTAL COMPOSITENESS AS INPUT

Here we apply the formalism derived in Secs. II and III to study the nature of the resonances  $f_0(980)$  and  $a_0(980)$ . Subsequently, the former method based on the saturation of  $\Gamma_R$  and  $X$  is denoted by S, while the latter one based on the use of a Flatté parameterization is called F. For each resonance pole we first apply the method S and then F.

##### A. The $f_0(980)$ resonance

Assuming given values for the total compositeness  $X$  of the  $f_0(980)$ , varying it from 0.2 to 0.8 in steps of 0.2, we obtain the couplings, partial-decay widths, and compositeness coefficients by solving Eq. (11) and Eq. (14). As already mentioned, we consider the RS II where  $s_R$  of Eq. (9) lies [77] and the results calculated are shown in Table I. One can observe from this table that the compositeness coefficient  $X_2$  is always much larger than  $X_1$ , which means that the  $K\bar{K}$  channel plays a much more important role than the  $\pi\pi$  one in the structure of  $f_0(980)$ . Related to this point, the  $f_0(980)$  couples much more strongly to  $K\bar{K}$  than to  $\pi\pi$ , in agreement with the fact that  $f_0(980)$  sits very close to the  $K\bar{K}$  threshold. We also observe from Table I that as the total compositeness  $X$  increases the physical partial-decay width to  $\pi\pi$  ( $\Gamma_{\pi\pi}$ ) decreases, while that to  $K\bar{K}$  becomes larger. Similarly, this fact has also been found in other heavy-quark resonances with open and near-threshold channels [66–68, 93]. In these regards, it follows from Table I that  $\Gamma_{K\bar{K}} > \Gamma_{\pi\pi}$  for  $X \gtrsim 0.6$ ,<sup>3</sup> but as  $X$  decreases  $\Gamma_{\pi\pi}$  becomes larger than  $\Gamma_{K\bar{K}}$ .

For estimating the errors associated to the input values of the resonance pole mass and width we proceed in this work similarly as done in Ref. [63]. Then, we discretize the inputs,  $m_R$  and  $\Gamma_R$  from the pole position at several points within one standard deviation region from the central values to generate a data grid. For each of the points in the grid we proceed to calculate the

---

<sup>3</sup> This can be easily seen because  $\Gamma_{K\bar{K}} > 25$  MeV.

different outputs so that their central values correspond to the mean values and the errors to the square root of the variances. We have also checked that this procedure is (of course) stable if the number of points in the grid is increased. For the other input  $X$  the variation in the results calculated for the different values of  $X$  provides an estimate of this source of uncertainty.

TABLE I. Method S applied to the resonance  $f_0(980)$  with pole position in the RS II (column 2) from Ref. [77], Eq. (9): The couplings  $|\gamma_i|$  (columns 3, 4), corresponding partial-decay widths  $\Gamma_i$  (columns 5, 6), and individual compositeness coefficients  $X_i$  (columns 7, 8) are calculated for  $X = 0.8, 0.6, 0.4, 0.2$  (column 1).

$X$	RS	$ \gamma_{\pi\pi} (\text{GeV})$	$ \gamma_{K\bar{K}} (\text{GeV})$	$\Gamma_1(\text{MeV})$	$\Gamma_2(\text{MeV})$	$X_{\pi\pi}$	$X_{K\bar{K}}$
0.80	II	$2.24 \pm 0.20$	$4.65 \pm 0.23$	$97.2 \pm 16.9$	$43.2 \pm 8.4$	$0.038 \pm 0.007$	$0.762 \pm 0.007$
0.60	II	$2.11 \pm 0.19$	$4.01 \pm 0.19$	$86.1 \pm 14.8$	$32.1 \pm 6.2$	$0.033 \pm 0.006$	$0.567 \pm 0.006$
0.40	II	$1.97 \pm 0.17$	$3.24 \pm 0.15$	$75.0 \pm 12.9$	$21.0 \pm 4.0$	$0.029 \pm 0.005$	$0.371 \pm 0.005$
0.20	II	$1.82 \pm 0.16$	$2.23 \pm 0.09$	$63.9 \pm 11.0$	$9.9 \pm 1.8$	$0.025 \pm 0.004$	$0.175 \pm 0.004$

We now consider the application of the method F, take  $X = 0.2$  to  $0.8$  in steps of  $0.2$ , and calculate the parameters characterizing the Flatté formula, Eq. (17), that is, the bare width to the lighter channel  $\tilde{\Gamma}_1$ , the bare coupling squared  $g_2$  to  $K\bar{K}$  and  $E_f$ . As typical outputs we provide  $\Gamma_1$ ,  $\Gamma_2$ ,  $X_1$  and  $X_2$ . For the pole position of the  $f_0(980)$  we take Eq. (9), with the results given in Table II.

Comparing the values of  $X_2$  for the  $f_0(980)$  between Table II and the previous Table I we see a good agreement, with the difference in the central values affecting the third decimal figure. This close agreement can be explained, though not completely, by noticing that  $X_2 \gg X_1$  so that  $X_2 \approx X$ , which fixes it to lie very close to the total compositeness. Regarding the  $\Gamma_i$  we see that they are very close between both tables for  $X = 0.2, 0.4$  and  $0.6$ , with larger differences for  $X = 0.8$ , but perfectly compatible within errors for all values of  $X$ . Let us notice that the method based on the Flatté parameterization directly provides  $\Gamma_i$ , since  $\Gamma_1 = \tilde{\Gamma}_1\beta$  and  $\Gamma_2 = \Gamma_1 - \Gamma_R$  for a pole in the RS II, as it is the case here for the  $f_0(980)$  poles in Eqs. (9) and (10). However, the method S in Sec. II keeps some spurious dependence on the value given to  $n$  for Eq. (13).

We now move on and consider the  $f_0(980)$  pole position from Ref. [74] given in Eq. (10), and proceed similarly as done regarding the pole position in Eq. (9). Then, we reproduce the values of the mass and width of the resonance in Eq. (10) together with a value given for  $X$ . The results obtained are shown in Table III.

Comparing Tables I and III we observe that all the outputs are rather similar. In particular the

TABLE II. Method F applied to the resonance  $f_0(980)$  with pole position in the RS II (column 2) from Ref. [77], Eq. (9): The value of  $X$  taken as input is given in the first column. We calculate the bare width  $\tilde{\Gamma}_1$  (column 3), the bare coupling  $g_2$  (column 4),  $E_f$  (column 5),  $\Gamma_1$  (column 6),  $\Gamma_2$  (column 7),  $X_1$  (column 8), and  $X_2$  (column 9).

$X$	RS	$\tilde{\Gamma}_{\pi\pi}(\text{MeV})$	$g_2$	$E_f(\text{MeV})$	$\Gamma_1(\text{MeV})$	$\Gamma_2(\text{MeV})$	$X_{\pi\pi}$	$X_{K\bar{K}}$
0.8	II	$948.3 \pm 383.1$	$110.01 \pm 4.03$	$-389.7 \pm 210.7$	$84.4 \pm 15.3$	$30.4 \pm 8.3$	$0.033 \pm 0.006$	$0.767 \pm 0.006$
0.6	II	$200.3 \pm 38.5$	$1.63 \pm 0.23$	$-57.6 \pm 19.3$	$80.4 \pm 14.4$	$26.4 \pm 7.0$	$0.031 \pm 0.006$	$0.569 \pm 0.006$
0.4	II	$113.2 \pm 20.1$	$0.66 \pm 0.07$	$-20.4 \pm 8.6$	$73.2 \pm 12.9$	$19.2 \pm 4.9$	$0.028 \pm 0.005$	$0.372 \pm 0.005$
0.2	II	$75.2 \pm 13.0$	$0.24 \pm 0.02$	$-4.2 \pm 5.3$	$63.9 \pm 11.1$	$9.9 \pm 2.4$	$0.025 \pm 0.004$	$0.175 \pm 0.004$

resulting values for  $X_2$  are almost coincident in both Tables, with  $X_2 \gg X_1$ . However, we notice that while the central value of the width for the pole in Eq. (9) is smaller than that in the pole of Eq. (10), the calculated  $\Gamma_1$  and  $\Gamma_2$  in Table I are larger than those in Table III. This indicates that the cancellation between widths in the difference  $\Gamma_1 - 2\Gamma_2$  for calculating the actual width to  $\pi\pi$  is more important in the pole of Eq. (9) than for the one in Eq. (10).

TABLE III. Method S applied to the resonance  $f_0(980)$  with pole position in the RS II from Ref. [74], Eq. (10). The various entries are the same as in Table I.

$X$	RS	$ \gamma_{\pi\pi} (\text{GeV})$	$ \gamma_{K\bar{K}} (\text{GeV})$	$\Gamma_1(\text{MeV})$	$\Gamma_2(\text{MeV})$	$X_{\pi\pi}$	$X_{K\bar{K}}$
0.80	II	$2.09 \pm 0.26$	$4.88 \pm 0.30$	$86.5 \pm 20.8$	$30.5 \pm 10.0$	$0.034 \pm 0.008$	$0.766 \pm 0.008$
0.60	II	$2.00 \pm 0.24$	$4.21 \pm 0.26$	$78.6 \pm 18.4$	$22.6 \pm 7.4$	$0.031 \pm 0.007$	$0.569 \pm 0.007$
0.40	II	$1.89 \pm 0.22$	$3.40 \pm 0.20$	$70.8 \pm 16.0$	$14.1 \pm 4.8$	$0.028 \pm 0.006$	$0.372 \pm 0.006$
0.20	II	$1.79 \pm 0.20$	$2.33 \pm 0.13$	$62.9 \pm 13.7$	$6.9 \pm 2.2$	$0.025 \pm 0.005$	$0.175 \pm 0.005$

For the method F the results are given in Table IV. We observe that the values of  $X_2$  obtained are very similar to those given in Table III for the same input  $X$ , with  $X_2 \gg X_1$ . The output  $\Gamma_2$  is smaller now than that in Table III, though within errors they are again compatible. This clearly indicates the compatibility between the two methods for this  $f_0(980)$  pole too. We also point out that the bare parameters for  $X = 0.8$  in Table IV are essentially undetermined, as indicated by the large intervals given between parenthesis, though the physical outputs appear with an uncertainty of similar size as that in the other rows of the table.

TABLE IV. Method F applied to the resonance  $f_0(980)$  with the pole position in the RS II from Ref. [74], Eq. (10). The various entries are the same as in Table II. The numbers between parenthesis indicate huge range of values of the corresponding quantity by varying  $m_R$  and  $\Gamma_R$  within errors.

$X$	RS	$\tilde{\Gamma}_{\pi\pi}$ (MeV)	$g_2$	$E_f$ (MeV)	$\Gamma_1$ (MeV)	$\Gamma_2$ (MeV)	$X_{\pi\pi}$	$X_{K\bar{K}}$
0.8	II	(430, $3 \cdot 10^6$ )	(5.4, $4 \cdot 10^4$ )	(-160, $-2 \cdot 10^6$ )	$71.6 \pm 18.2$	$16.8 \pm 7.9$	$0.028 \pm 0.007$	$0.772 \pm 0.007$
0.6	II	$218.4 \pm 51.9$	$2.34 \pm 0.52$	$-131.6 \pm 52.3$	$68.8 \pm 16.9$	$12.8 \pm 7.0$	$0.027 \pm 0.007$	$0.573 \pm 0.007$
0.4	II	$113.6 \pm 25.1$	$0.83 \pm 0.13$	$-52.6 \pm 20.7$	$65.6 \pm 15.4$	$9.6 \pm 5.1$	$0.026 \pm 0.006$	$0.374 \pm 0.006$
0.2	II	$75.2 \pm 16.1$	$0.27 \pm 0.03$	$-24.2 \pm 11.8$	$61.1 \pm 13.6$	$5.1 \pm 2.6$	$0.024 \pm 0.005$	$0.176 \pm 0.005$

### B. The $a_0(980)$ resonance

Let us explore the compositeness of the  $a_0(980)$  similarly as done above in Sec. IV A for the  $f_0(980)$ . The poles that we are going to consider next for the  $a_0(980)$  stems from a recent coupled-channel partial-wave analysis of antiproton-proton annihilation data in Ref. [71], where the pole parameters and the partial-decay width of the  $a_0(980)$  are discussed. In the RS II Ref. [71] reports the values

$$m_{a_0} = 1004.1 \pm 6.67 \text{ MeV}, \quad \Gamma_{a_0} = 97.2 \pm 6.01 \text{ MeV}, \quad \Gamma_{K\bar{K}}/\Gamma_{\pi\eta} = (13.8 \pm 3.5) \%, \quad (55)$$

while in the RS III the same reference provides

$$m_{a_0} = 1002.4 \pm 6.55 \text{ MeV}, \quad \Gamma_{a_0} = 127.0 \pm 7.08 \text{ MeV}, \quad \Gamma_{K\bar{K}}/\Gamma_{\pi\eta} = (14.9 \pm 3.9) \%, \quad (56)$$

with the uncertainties added in quadrature.

Let us denote by 1 the lighter channel  $\pi\eta$ , and by 2 the heavier one  $K\bar{K}$ . Combining Eq. (11) for the total compositeness and Eq. (14) for the full width, given input values for the former between 0.2 and 0.8 in steps of 0.2, we derive a series of partial compositeness coefficients and decay widths for the  $a_0(980)$  in Table V by applying the method S.<sup>4</sup> We find that  $X_2$  is rather similar for the RS II and III calculations. We also obtain that  $X_2 \gg X_1$ , except for  $X = 0.2$  in which case they are quite close to each other. This tells us that the  $K\bar{K}$  component typically dominates over the  $\pi\eta$  one for the resonance  $a_0(980)$ .

The results corresponding to the method F for the  $a_0(980)$  case are organized in Table VI. One then finds that the values of  $X_2$  obtained in Tables VI and V are very close independently of the

<sup>4</sup> The same remark as for the  $f_0(980)$  in the footnote 1 can also be applied for the  $a_0(980)$  when its pole is taken in the RS II for applying Eq. (1) to calculate  $X_2$ . The point is that the  $a_0(980)$  mass in Eq. (55) is clearly larger than the  $K\bar{K}$  threshold but the width of the resonance is much larger than the difference between  $m_{a_0}$  and the  $K\bar{K}$  threshold.

TABLE V. Method S applied for the resonance  $a_0(980)$  with pole positions from Ref. [71], Eqs. (55) and (56), in different RSs (column 2): We take input values for  $X$  (column 1), and predict  $|\gamma_i|$  (columns 3, 4),  $\Gamma_i$  (columns 5, 6), and  $X_i$  (columns 7, 8).

$X$	RS	$ \gamma_{\pi\eta} (\text{GeV})$	$ \gamma_{K\bar{K}} (\text{GeV})$	$\Gamma_1(\text{MeV})$	$\Gamma_2(\text{MeV})$	$X_{\pi\eta}$	$X_{K\bar{K}}$
0.8	II	$3.57 \pm 0.07$	$5.15 \pm 0.04$	$169.1 \pm 7.0$	$71.9 \pm 4.9$	$0.151 \pm 0.005$	$0.649 \pm 0.005$
	III	$2.30 \pm 0.09$	$4.50 \pm 0.06$	$70.4 \pm 5.5$	$56.6 \pm 4.4$	$0.064 \pm 0.006$	$0.736 \pm 0.006$
0.6	II	$3.35 \pm 0.06$	$4.37 \pm 0.03$	$149.0 \pm 5.8$	$51.8 \pm 5.8$	$0.133 \pm 0.005$	$0.467 \pm 0.005$
	III	$2.56 \pm 0.07$	$3.78 \pm 0.05$	$86.9 \pm 4.9$	$40.1 \pm 3.1$	$0.079 \pm 0.005$	$0.521 \pm 0.005$
0.4	II	$3.12 \pm 0.05$	$3.41 \pm 0.02$	$128.8 \pm 4.6$	$31.6 \pm 2.2$	$0.115 \pm 0.004$	$0.285 \pm 0.004$
	III	$2.79 \pm 0.06$	$2.90 \pm 0.04$	$103.5 \pm 4.5$	$23.5 \pm 1.9$	$0.094 \pm 0.005$	$0.306 \pm 0.005$
0.2	II	$2.86 \pm 0.05$	$2.05 \pm 0.01$	$108.6 \pm 3.7$	$11.4 \pm 0.8$	$0.097 \pm 0.003$	$0.103 \pm 0.003$
	III	$3.01 \pm 0.06$	$1.58 \pm 0.04$	$120.0 \pm 4.5$	$7.0 \pm 0.7$	$0.109 \pm 0.005$	$0.091 \pm 0.005$

TABLE VI. Method F applied to the resonance  $a_0(980)$  with pole positions from Ref. [71], Eqs. (55) and (56), in different RSs (column 2): We calculate the bare width  $\tilde{\Gamma}_1$  (column 3), the bare coupling squared  $g_2$  (column 4),  $E_f$  (column 5),  $\Gamma_1$  (column 6),  $\Gamma_2$  (column 7),  $X_1$  (column 8) and  $X_2$  (column 9). The value of  $X$  taken as input is given in the first column.

$X$	RS	$\tilde{\Gamma}_{\pi\eta}(\text{MeV})$	$g_2$	$E_f(\text{MeV})$	$\Gamma_1(\text{MeV})$	$\Gamma_2(\text{MeV})$	$X_{\pi\eta}$	$X_{K\bar{K}}$
0.8	II	$740.5 \pm 42.2$	$5.16 \pm 0.51$	$-237.1 \pm 39.4$	$157.2 \pm 8.8$	$60.0 \pm 7.4$	$0.141 \pm 0.007$	$0.659 \pm 0.007$
	III	$35.9 \pm 7.3$	$0.66 \pm 0.03$	$49.3 \pm 4.6$	$45.6 \pm 9.7$	$81.4 \pm 9.3$	$0.042 \pm 0.009$	$0.758 \pm 0.009$
0.6	II	$289.7 \pm 8.5$	$1.54 \pm 0.06$	$-61.6 \pm 10.0$	$146.2 \pm 7.2$	$49.0 \pm 5.6$	$0.131 \pm 0.005$	$0.469 \pm 0.005$
	III	$59.9 \pm 5.6$	$0.49 \pm 0.02$	$39.2 \pm 4.3$	$72.7 \pm 7.1$	$54.3 \pm 6.2$	$0.066 \pm 0.007$	$0.534 \pm 0.007$
0.4	II	$177.4 \pm 5.6$	$0.64 \pm 0.01$	$-18.2 \pm 5.8$	$129.9 \pm 5.4$	$32.7 \pm 3.5$	$0.116 \pm 0.004$	$0.284 \pm 0.004$
	III	$85.2 \pm 4.7$	$0.30 \pm 0.01$	$28.6 \pm 4.1$	$96.9 \pm 5.3$	$30.1 \pm 3.4$	$0.089 \pm 0.006$	$0.311 \pm 0.006$
0.2	II	$120.2 \pm 3.8$	$0.18 \pm 0.002$	$4.0 \pm 4.3$	$109.9 \pm 3.8$	$12.7 \pm 1.4$	$0.099 \pm 0.003$	$0.101 \pm 0.003$
	III	$113.6 \pm 4.6$	$0.10 \pm 0.01$	$16.7 \pm 4.0$	$118.6 \pm 4.6$	$8.4 \pm 1.1$	$0.108 \pm 0.005$	$0.092 \pm 0.005$

RS in which the poles lie. It turns out that  $X_2$  is typically much larger than  $X_1$  except when  $X$  becomes small, like  $X = 0.2$  in Table VI, and then both  $X_i$  are rather close to each other. Regarding the  $\Gamma_i$  it is clear that for the pole in the RS II the values obtained now in Table VI are remarkably similar to those in Table V. However, they clearly differ for  $X \geq 0.8$  for the RS III

case.

As indicated above one should distinguish between the bare and dressed parameters in a Flatté parameterization. This reflects in the fact that the bare width  $\tilde{\Gamma}_1$  can be much larger than the total width  $\Gamma_R$ . This is particularly true when the pole position is set to lie in the RS II, as it is clear from the Tables II, IV and VI. Here in addition one has to properly relate  $\Gamma_1$  and  $\Gamma_{\pi\pi}$ , cf. Eq. (43). Nonetheless, these important points have been overlooked in the literature.

Before finishing this section we should mention that in some studies the  $a_0(980)$  lies in the RS IV, so that there is no an interval along the physical real- $s$  axis within the radius of convergence of the Laurent series around the  $a_0(980)$ . In such a scenario it is not justified to apply Eq. (1) for the calculation of  $X_2$ , as discussed in detail in Ref. [61], and it is not either clear how to connect the  $\Gamma_i$  with the physical partial-decay widths. Then, it follows that our method cannot be applied and the conclusions thereof do not hold. In the studies based on unitarization of SU(3) and U(3) Chiral Perturbation Theory it is observed that the pole for the  $a_0(980)$  appears in the 2nd RS if only tree level amplitudes are kept. This is necessarily the case when unitarizing the leading order amplitudes [25, 28, 42, 72]. However, once loop contributions are accounted for the pole moves to the RS IV [72, 74, 94]. This is also the case in the  $K$ -matrix analysis of Ref. [73]. The more recent studies among those quoted here [72, 73] also reproduce the energy levels from lattice QCD simulations. When the  $a_0(980)$  lies in the RS IV it manifests on the physical real- $s$  axis as a strong cusp effect.

## V. RESULTS AND DISCUSSIONS USING THE BRANCHING RATIO $r_{\text{exp}}$ AS INPUT

Here, we directly explore the more stringent scenario of taking  $r_{\text{exp}}$ , together with the usual reproduction of the pole position  $E_R$ , in order to fix all the parameters both in the S and F methods. The direct consideration of  $r_{\text{exp}}$  as input is an interesting check on the consistency of interpreting the  $\Gamma_i$ , calculated from the pole parameters, in connection with the experimental  $r_{\text{exp}}$  for a pole lying in the RS II. As shown below, the resulting physical-partial-decay widths have values within meaningful ranges, such that they are positive and smaller than the total width, while the  $X_i$  and their sum  $X$  also lie within the allowed interval  $[0, 1]$ .<sup>5</sup> This situation is similar to the one obtained before when taking  $X$  as input, where all the Flatté parameters are fixed without the need to connect the  $\Gamma_i$  with  $r_{\text{exp}}$ , which comes out as an output.

We also show below that the procedure of providing  $r_{\text{exp}}$  as input is not completely satisfactory because the output value for the renormalized coupling squared to  $K\bar{K}$ ,  $|\gamma_2|^2$ , can be very sensitive

<sup>5</sup> Otherwise, if not correctly understanding  $r_{\text{exp}}$  as proposed for a RS II pole, there will be no solution within the method F developed in Sec. III.

to small variations in the input. As a result, the calculation of  $X_2$  by using Eq. (1) does not come out very accurate, particularly for the  $f_0(980)$ . We can circumvent this limitation by then using the method of the spectral function  $\omega(E)$  to estimate  $X$  with better precision. With this choice we also update values for the resonance inputs compared with the original Ref. [55], in which the use of the spectral density function to calculate the compositeness was applied for the first time to the  $f_0(980)$  and  $a_0(980)$  resonances.

### A. The $f_0(980)$ resonance

Now, let us directly combine the knowledge of  $E_R$  with the input for the branching ratio  $r_{\text{exp}}$ ,  $r_{\text{exp}} = 0.52 \pm 0.12$  [70] and  $r_{\text{exp}} = 0.75_{-0.13}^{+0.11}$  [95], as well as  $r_{\text{exp}} = 0.68$  from the theoretical analysis of Ref. [25].

We start by applying the method S. It is clear that given  $r_{\text{exp}}$  and  $\Gamma_R$  one can solve for the couplings  $|\gamma_i|$ ,  $i = 1, 2$ , and calculate the partial compositeness coefficients  $X_i$ . Since the  $f_0(980)$  poles that we are considering lie in the RS II we have that  $\Gamma_{\pi\pi} = (2 - r_{\text{exp}})\Gamma_R$  and  $\Gamma_{K\bar{K}} = (1 - r_{\text{exp}})\Gamma_R$ , and similarly for the RS II pole for the  $a_0(980)$ ,  $\Gamma_{\pi\eta} = (2 - r_{\text{exp}})\Gamma_R$ . For the  $a_0(980)$  pole in the RS III we have instead  $\Gamma_{\pi\eta} = r_{\text{exp}}\Gamma_R$ . By combining Eqs. (1), (12) and (13) the value of the compositeness coefficients  $X_1$  and  $X_2$  can be written as

$$X_1 = \frac{8\pi(2 - r_{\text{exp}})\Gamma_R m_R^2}{p_1(m_R^2)} \left| \frac{\partial G_1(s)}{\partial s} \right|_{s=s_R}, \text{ RS II}, \quad (57)$$

$$X_1 = \frac{8\pi r_{\text{exp}}\Gamma_R m_R^2}{p_1(m_R^2)} \left| \frac{\partial G_1(s)}{\partial s} \right|_{s=s_R}, \text{ RS III},$$

$$X_2 = \frac{16\pi^2(1 - r_{\text{exp}})\Gamma_R}{\int_{m_1+m_2}^{m_R+2\Gamma_R} dW \frac{p(W^2)/W^2}{(m_R-W)^2 + \Gamma_R^2/4}} \left| \frac{\partial G_2(s)}{\partial s} \right|_{s=s_R}. \quad (58)$$

The results are organized in Table VII with  $m_R$  and  $\Gamma_R$  taken from Eq. (9), corresponding to the determination in Ref. [77]. For this and the rest of tables in this section the errorbars given to  $X_2$  and  $X$  contain also the propagation of the error in the determination of  $r_{\text{exp}}$  from Refs. [70, 95]. It follows from this table that  $X_2$  is affected by large errorbars, around a 50%, so that the resulting  $X$  is not pinned down accurately and the calculation is rather indicative. Only for  $r_{\text{exp}} = 0.52 \pm 0.12$  [70] one has that  $X$  can be larger than 0.5 within errors, with  $X = 0.49 \pm 0.20$ . For the other experimental value  $r_{\text{exp}} = 0.75_{-0.13}^{+0.11}$  [95] the compositeness  $X = 0.27 \pm 0.11$  and it is smaller than 0.5.

We show in the left panel of Fig. 1 the total compositeness  $X$  as a function of  $r_{\text{exp}}$  for the  $f_0(980)$  with the method S, and employing the central values for  $m_R$  and  $\Gamma_R$  for the different poles considered. Thus, the requirement that  $r_{\text{exp}} > 0.4$  implies that  $X \lesssim 0.6$  for the pole in Eq. (9)

in the RS II. It is also clear from Fig. 1 the linear decrease of  $X$  with  $r_{\text{exp}}$ . This can be easily understood by noticing that both the partial-decay widths and partial compositeness coefficients are proportional to  $|\gamma_i|^2$ , which can be written in turn as  $\Gamma_i/\theta_i$ . For given values for the mass and width of the resonance the  $\theta_i$  is just a measure of the available phase space for the decay to the channel  $i$ , and then  $\theta_2 \ll \theta_1$ . In this way, for a pole in the RS III,

$$\begin{aligned} X &= \frac{\Gamma_R r_{\text{exp}}}{\theta_1} \left| \frac{\partial G_1}{\partial s} \right|_{s=s_R} + \frac{\Gamma_R (1 - r_{\text{exp}})}{\theta_2} \left| \frac{\partial G_2}{\partial s} \right|_{s=s_R} \\ &= \frac{\Gamma_R}{\theta_2} \left| \frac{\partial G_2}{\partial s} \right|_{s=s_R} - r_{\text{exp}} \Gamma_R \left( \frac{1}{\theta_2} \left| \frac{\partial G_2}{\partial s} \right|_{s=s_R} - \frac{1}{\theta_1} \left| \frac{\partial G_1}{\partial s} \right|_{s=s_R} \right). \end{aligned} \quad (59)$$

This is a linear dependence with  $r_{\text{exp}}$ , and the coefficient multiplying the latter is negative because both  $1/\theta_2$  and  $|\partial G_2/\partial s|_{s_R}$  are basically proportional to  $|s_R/4 - m_K^2|^{-1/2}$ , cf. Eq. (38).<sup>6</sup>

TABLE VII. Method S applied to the resonance  $f_0(980)$  with pole position in the RS II (column 2) from Ref. [77], Eq. (9): By reproducing values given for  $r_{\text{exp}}$  (column 1), we calculate  $|\gamma_i|$  (columns 3, 4),  $\Gamma_i$  (columns 5, 6), and  $X_i$  (columns 7, 8).

$r_{\text{exp}}$	RS	$ \gamma_1 (\text{GeV})$	$ \gamma_2 (\text{GeV})$	$\Gamma_1(\text{MeV})$	$\Gamma_2(\text{MeV})$	$X_{\pi\pi}$	$X_{K\bar{K}}$
0.52 [70]	II	$2.03 \pm 0.18$	$3.62 \pm 0.32$	$79.9 \pm 14.5$	$25.9 \pm 4.7$	$0.031 \pm 0.006$	$0.46 \pm 0.20$
0.68 [25]	II	$1.92 \pm 0.17$	$2.95 \pm 0.26$	$71.3 \pm 13.0$	$17.3 \pm 3.1$	$0.028 \pm 0.005$	$0.31 \pm 0.13$
0.75 [95]	II	$1.87 \pm 0.17$	$2.61 \pm 0.23$	$67.5 \pm 12.3$	$13.5 \pm 2.5$	$0.026 \pm 0.005$	$0.24 \pm 0.11$

<sup>6</sup> Eq. (59) was written for a pole in the RS III. For a pole lying in the RS II one has to take into account that  $\Gamma_1 = \Gamma_R(2 - r_{\text{exp}})$  and, then, instead of Eq. (59) we have

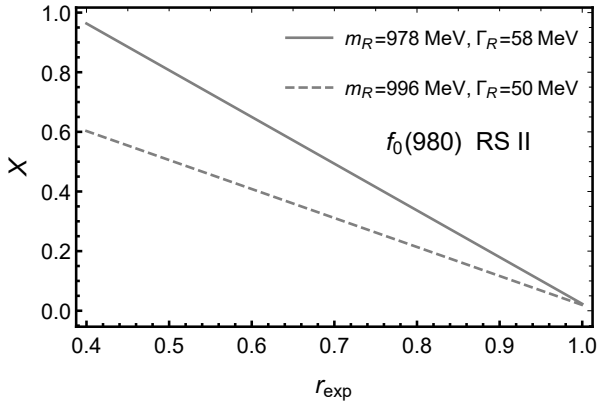
$$X = 2 \frac{\Gamma_R}{\theta_1} \left| \frac{\partial G_1}{\partial s} \right|_{s=s_R} + \frac{\Gamma_R}{\theta_2} \left| \frac{\partial G_2}{\partial s} \right|_{s=s_R} - r_{\text{exp}} \Gamma_R \left( \frac{1}{\theta_2} \left| \frac{\partial G_2}{\partial s} \right|_{s=s_R} + \frac{1}{\theta_1} \left| \frac{\partial G_1}{\partial s} \right|_{s=s_R} \right), \quad (60)$$

so that the linear decrease of  $X$  with  $r_{\text{exp}}$  follows.

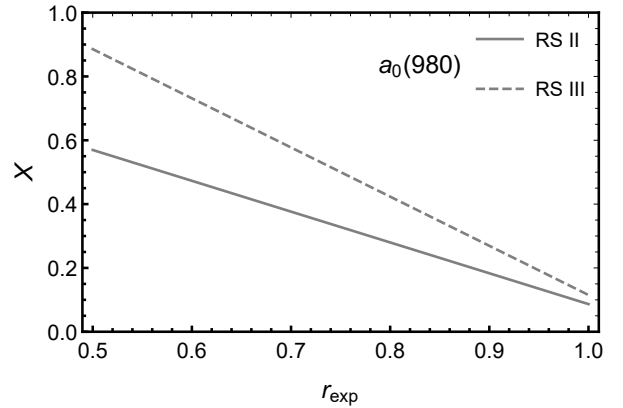
TABLE VIII. Method F applied to the resonance  $f_0(980)$  with the pole position in the RS II from Ref. [77], Eq. (9): The branching ratio  $r_{\text{exp}}$  is taken as input (column 1). We then calculate the bare partial-decay width  $\tilde{\Gamma}_1$  (column 2), the bare coupling squared  $g_2$  (column 3),  $E_f$  (column 4), the renormalized  $\Gamma_1$  (column 5) and  $\Gamma_2$  (column 6), and the partial compositeness coefficients  $X_1$  (column 7) and  $X_2$  (column 8). The numbers between parenthesis indicate large ranges of the corresponding quantities by varying  $m_R$  and  $\Gamma_R$  within errors.

$r_{\text{exp}}$	$\tilde{\Gamma}_{\pi\pi}$ (MeV)	$g_2$	$E_f$ (MeV)	$\Gamma_1$ (MeV)	$\Gamma_2$ (MeV)	$X_{\pi\pi}$	$X_{K\bar{K}}$
0.52 [70]	(71, 2623)	(0.36, 26.8)	(-21.2, 1167.2)	$79.9 \pm 14.5$	$25.9 \pm 4.7$	$0.030 \pm 0.006$	$0.48 \pm 0.22$
0.68 [25]	$113.8 \pm 38.3$	$0.69 \pm 0.45$	(-66.7, 6.3)	$71.3 \pm 13.0$	$17.3 \pm 3.1$	$0.028 \pm 0.005$	$0.35 \pm 0.18$
0.75 [95]	$89.4 \pm 20.4$	$0.41 \pm 0.17$	(-42.9, 7.7)	$67.5 \pm 12.3$	$13.5 \pm 2.5$	$0.026 \pm 0.005$	$0.26 \pm 0.14$

FIG. 1. The total compositeness  $X$  is plotted as a function of the input branching ratio ( $r_{\text{exp}}$ ) when applying the method S. Panel (a) corresponds to the  $f_0(980)$ : The dashed line is for the pole from Ref. [77], Eq. (9), and the dashed one is for the pole of Ref. [74], Eq. (10). Panel (b) corresponds to the  $a_0(980)$ : The poles for the  $a_0(980)$  are given in Eqs. (55) and (56) for the RSs II and III, respectively, and they are taken from Ref. [71].



(a)



(b)

Now we apply the method F with  $r_{\text{exp}}$  as input to the same  $f_0(980)$  pole given in Eq. (9), and the results are presented in the Table VIII. In the columns 2–4 we provide the resulting parameters characterizing the Flatté parameterization, and in the rest of columns we calculate the outputs in

the form of the partial-decay widths  $\Gamma_i$  and partial compositeness coefficients  $X_i$ . We notice that for the smallest  $r_{\text{exp}} = 0.52$  [70] the bare parameters are much more poorly determined than those in the other cases. Nonetheless, the outputs have uncertainties of similar sizes as for the other values taken for  $r_{\text{exp}}$ . The resulting values for  $X_2$  in Tables VIII and VII turn out to be remarkably close to each other, clearly showing the compatibility between the methods F and S.

Let us compare Table VIII with Table II, where  $X$  is taken as input and no use of the interpretation of the  $\Gamma_i$  for a pole in the RS II, according to Eq. (43), is done to fix the Flatté parameterization. One can then observe that similar values of  $\Gamma_{K\bar{K}}$ , which fixes  $r_{\text{exp}} = 1 - \Gamma_{K\bar{K}}/\Gamma_R$ , lead to close values of  $X_2$  in both tables. This agreement is of course an indication that the equations are correctly solved, because the same results are obtained by taking corresponding values of  $X$  or  $r_{\text{exp}}$ .

TABLE IX. Method S applied to the resonance  $f_0(980)$  with pole position in the RS II from Ref. [74], Eq. (10). The various entries are the same as in Table VII.

$r_{\text{exp}}$	RS	$ \gamma_{\pi\pi} (\text{GeV})$	$ \gamma_{K\bar{K}} (\text{GeV})$	$\Gamma_1(\text{MeV})$	$\Gamma_2(\text{MeV})$	$X_{\pi\pi}$	$X_{K\bar{K}}$
0.52 [70]	II	$2.05 \pm 0.22$	$4.71 \pm 0.70$	$82.9 \pm 18.2$	$26.9 \pm 5.9$	$0.033 \pm 0.007$	$0.72 \pm 0.34$
0.68 [25]	II	$1.94 \pm 0.21$	$3.85 \pm 0.58$	$73.9 \pm 16.2$	$17.9 \pm 3.9$	$0.029 \pm 0.006$	$0.48 \pm 0.23$
0.75 [95]	II	$1.88 \pm 0.21$	$3.40 \pm 0.51$	$70.0 \pm 15.3$	$14.0 \pm 3.1$	$0.027 \pm 0.006$	$0.38 \pm 0.18$

TABLE X. Method F applied to the resonance  $f_0(980)$  with the pole position in the RS II from Ref. [74], Eq. (10): The entries are the same as those in Table VIII, except for the values of  $r_{\text{exp}}$  in the first column because solutions are found only for  $r_{\text{exp}} > 0.82$ . The values of  $r_{\text{exp}}$  taken do not come from any experiment and are considered due to theoretical reasons.

$r_{\text{exp}}$	$\tilde{\Gamma}_{\pi\pi}(\text{MeV})$	$g_2$	$E_f(\text{MeV})$	$\Gamma_1(\text{MeV})$	$\Gamma_2(\text{MeV})$	$X_{\pi\pi}$	$X_{K\bar{K}}$
0.86	(45.8, 2632)	(0.13, 35.6)	(-2358, 0.3)	$63.8 \pm 14.0$	$7.8 \pm 1.7$	$0.026 \pm 0.005$	$0.329 \pm 0.140$
0.91	(41.9, 407.6)	(0.08, 6.64)	(-429.4, 1.3)	$61.0 \pm 13.4$	$5.1 \pm 1.1$	$0.025 \pm 0.005$	$0.239 \pm 0.123$
0.96	$66.1 \pm 13.0$	$0.16 \pm 0.12$	$-20.8 \pm 14.4$	$58.2 \pm 12.8$	$2.3 \pm 0.5$	$0.023 \pm 0.005$	$0.105 \pm 0.058$

Let us move on and consider the  $f_0(980)$  pole position from Ref. [74] applying first the method S, with the results given in Table IX. We already noticed when comparing Tables I and III that the  $\Gamma_i$ 's were larger for the former despite the width of the pole in Eq. (9) is smaller. By comparing Tables VII and IX with  $r_{\text{exp}}$  as input we observe that the partial-decay widths  $\Gamma_i$ 's have close

values between them and that the differences translates into the central values of  $X_2$ , which are always larger in Table IX than the ones in Table VII. Thus, a somewhat more prominent role of the  $K\bar{K}$  component in the case of the  $f_0(980)$  pole in Eq. (10) arises.

When applying the method F to the  $f_0(980)$  pole from Ref. [74], Eq. (10), there are no acceptable solutions for the input values of  $r_{\text{exp}}$  from Refs. [25, 70, 95], with solutions found only for larger values of  $r_{\text{exp}}$ . Indeed, we see from Eq. (45) that the central value for  $r_{\text{exp}}$  calculated from the information given in Ref. [74] is 0.91, though the error estimated is too large to extract more stringent quantitative conclusions. Our results are given in the Table X, where  $X_2$  varies by around a factor of 3 when changing  $r_{\text{exp}}$  by less than a 10%, from  $r_{\text{exp}} = 0.96$  to 0.86. For similar values of  $\Gamma_{K\bar{K}}$  the results now and those in Table IV agree well within errors, and give rise to rather small values for  $X_2$ .

Interestingly, we can check our procedure with the full characterization of the  $f_0(980)$  pole given in Ref. [74], in which the residues, in addition to the pole position, are given. In this reference one has  $|\gamma_1| = 1.8_{-0.3}^{+0.2}$  GeV and  $|\gamma_2/\gamma_1| = 2.6_{-0.3}^{+0.2}$ . Precisely, the input value for  $r_{\text{exp}} = 2 - \frac{\Gamma_1}{\Gamma_R} = 0.909$ , cf. Eq. (45), is equivalent to providing the central value of  $|\gamma_1|$  as input, and solving the equation

$$|\gamma_1|^2 = \beta g_1 = \beta \frac{\tilde{\Gamma}_1 8\pi m_R^2}{p_1(m_R)}, \quad (61)$$

instead of Eq. (44). The result is the same as the one given in the third row of Table X corresponding to a value  $|\gamma_2| = \sqrt{32\pi m_K^2 \beta g_2} = 2.77$  GeV (which straightforwardly translates into the central value for  $X_2$  by using Eq. (1)). We notice that this value is a factor of 1.7 smaller than the reported one in Ref. [74]. Its square is therefore a factor of 2.84 smaller than the value  $|\gamma_2|^2 = (4.68 \text{ GeV})^2$  actually obtained in Ref. [74] by solving for the residues of the partial-wave amplitudes.

However, instead of  $|\gamma_1|$  we can take  $|\gamma_2|$  as input and solve the equation

$$|\gamma_2|^2 = 32\pi m_K^2 \beta g_2, \quad (62)$$

instead of Eq. (61). Doing this exercise with the central value  $|\gamma_2| = 4.68$  GeV [74], corresponding to a much larger  $X_2 = 0.68$ , we find that  $|\gamma_1| = 1.875$  GeV, which is indeed perfectly compatible with the value  $|\gamma_1| = 1.8_{-0.3}^{+0.2}$  GeV given in Ref. [74]. The branching ratio  $r_{\text{exp}}$  obtained with this value of  $|\gamma_1|$  is 0.81, instead of 0.91 for  $|\gamma_1| = 1.8$  GeV (third row in Table X).<sup>7</sup>

<sup>7</sup> At first sight it could seem strange that  $|\gamma_1| = 1.875 > 1.8$  GeV has  $r_{\text{exp}} = 0.81 < 0.91$ , respectively. This is because for  $|\gamma_1| = 1.875$  GeV the coupling  $|\gamma_2| = 4.68 > 2.77$  GeV and the decay width to  $K\bar{K}$ ,  $\Gamma_1 - \Gamma_R$ , has increased. The fact that the width to  $K\bar{K}$  has not increased by a relative factor of 2.84 as  $|\gamma_2|^2$  does is a reflection of some divergence between the F and S methods for large  $K\bar{K}$  couplings in the case of the pole in Eq. (10). This point is also clear from the absence of solutions for  $r_{\text{exp}} = 0.52, 0.68$  and  $0.75$  within the method F, although they are found for the method S in Table IX. Some divergence in the results when taking  $X$  as input can also be seen for larger values of  $X \geq 0.6$  (and hence of  $|\gamma_2|$ ) by comparing the central values for the  $\Gamma_i$  between Tables III

After this check we re-consider the application of the method F to the  $f_0(980)$  pole in Eq. (9) and discuss the central values of  $|\gamma_1|$  ( $|\gamma_2|$ ) for the input values of  $r_{\text{exp}}$  in Table VIII. For the extreme values  $r_{\text{exp}} = 0.52$ , and  $0.75$  we find  $1.96$  ( $3.88$ ) GeV, and  $1.78$  ( $2.40$ ) GeV, respectively. With a small variation of a 5% in  $r_{\text{exp}}$ , between the values  $0.95r_{\text{exp}}$  and  $1.05r_{\text{exp}}$  the coupling squared  $|\gamma_2|^2$  changes by 16% for  $r_{\text{exp}} = 0.52$  and by 40% for  $r_{\text{exp}} = 0.75$ . This implies that though there is no a critical dependence of  $|\gamma_2|$  on the value of  $r_{\text{exp}}$  as in the case of the  $f_0(980)$  from Ref. [74], cf. Table X, it is also true that the variations are important. Considering the experimental errors in  $r_{\text{exp}}$  from Refs. [70, 95] of around a 23% for  $r_{\text{exp}} = 0.52$  and 15% for  $r_{\text{exp}} = 0.75$ , we have added in quadrature the resulting uncertainty of around a 40% in  $X_2$  to the one stemming from the values of  $M_R$  and  $\Gamma_R$  for calculating the errorbars in Table VIII.

A similar relative uncertainty, which also follows by inspection of the dashed line in the left panel of Fig. 1, has been applied to  $X_2$  in Table VII calculated with the method S. We have proceeded analogously for the errorbars of  $X_2$  shown in Table IX. Notice that within the method S the sensitivity to the input value of  $r_{\text{exp}}$  for the pole in Eq. (10) is a factor of 1.6 larger than for the pole in Eq. (9), as follows by comparing the slope of the solid versus the dashed lines in the left panel of Fig. 1.

We then find a rather unpleasant situation in which small changes in the input values, perfectly well within the errorbars provided by the analyses where they come from, can give rise to a very different output value for  $|\gamma_2|^2$  and then for  $X_2$ , the partial compositeness coefficient which typically almost saturates the whole  $X$ . A way that we have found to circumvent this limitation is to use the spectral density function  $\omega(E)$ , Eq. (47), in order to calculate the compositeness  $X$  as  $1 - W_R$ , since we have checked that it does not depend so sensitively on the input value of  $r_{\text{exp}}$ . In this regard, we calculate  $W_R$  as a function of the extent of the interval  $[-\Delta, \Delta]$  used in Eq. (47) because its dependence on  $\Delta$  is worth noticing, and the results for the  $f_0(980)$  pole in Eq. (10) are given in Table XI. In the first column we show the  $r_{\text{exp}}$  taken, the integration interval in Eq. (47) is given in the second column, the third column is for the resulting  $W_R$ , the fourth column provides  $1 - W_R$ , and the last one gives  $X$  calculated already with the method based on the Flatté parameterization in Table X.

In Ref. [55] the cutoff  $\Delta$  was taken to be 50 MeV. Since the width of the  $f_0(980)$  in Ref. [74] is 58 MeV we take  $\Delta = 60$  MeV for this pole, but estimate an uncertainty for the result of  $W_R$  by considering also  $\Delta = 90$  MeV, which is a 50% larger than the nominal value. This is illustrated in Fig. 2, where we plot  $\omega(E)$  for the  $f_0(980)$  and  $a_0(980)$  resonances in the top and bottom panels, respectively. It is clearly seen that most of the resonance bump lies in the region  $|E| < \Gamma_R$ , and that for  $|E| > 1.5\Gamma_R$  it has already faded away. From Table XI we obtain that for  $\Delta = 60$  MeV

and  $r_{\text{exp}} = 0.91$  (the nominal one for [74]) the resulting compositeness is  $1 - W_{f_0} = 0.52$ , and for  $\Delta = 1.5\Gamma_R \approx 90$  MeV, it decreases up to 0.43. We observe a variation of around a 40% for  $1 - W_{f_0}$  in Table XI calculated with  $\Delta = 60$  MeV (much smaller than the 300% in Table X), decreasing from 0.68 for  $r_{\text{exp}} = 0.86$  to 0.39 for  $r_{\text{exp}} = 0.96$ .

TABLE XI. Resonance  $f_0(980)$  with the pole position of Eq. (10) in the RS II: We show the dependence of  $W_{f_0}$  on the integration interval  $[-\Delta, \Delta]$  with  $\Delta$  up to  $2\Gamma_R$ . The last column gives  $X = X_1 + X_2$  obtained in Table X. The values of  $r_{\text{exp}}$  given do not come from any experiment and are considered due to theoretical reasons.

$r_{\text{exp}}$	$[-\Delta, \Delta]$	$W_{f_0}$	$1 - W_{f_0}$	$X$
0.86	$[-30, 30]$	0.19	0.81	
	$[-60, 60]$	0.32	0.68	
	$[-90, 90]$	0.40	0.60	
	$[-120, 120]$	0.45	0.55	$0.36 \pm 0.14$
0.91	$[-30, 30]$	0.30	0.70	
	$[-60, 60]$	0.48	0.52	
	$[-90, 90]$	0.57	0.43	
	$[-120, 120]$	0.63	0.37	$0.27 \pm 0.12$
0.96	$[-30, 30]$	0.40	0.60	
	$[-60, 60]$	0.61	0.39	
	$[-90, 90]$	0.71	0.29	
	$[-120, 120]$	0.76	0.24	$0.13 \pm 0.06$

Next, we apply the method based on the spectral density function  $\omega(E)$  to the pole from Ref. [77], Eq. (9), and the results are given in Table XII. The dependence with  $\Delta$  in the compositeness  $1 - W_{f_0}$  is indicated with the subscript  $\Delta$  in the fourth column of Table XII,  $(1 - W_{f_0})_\Delta$ . We take as the nominal value for  $1 - W_{f_0}$  the mean between the ones obtained with  $\Delta = \Gamma_R = 50$  MeV and  $\Delta = 1.5\Gamma_R$ . Considering the variation of the results between these two values for  $\Delta$ , and the errorbar of around 0.12 in  $r_{\text{exp}}$  in both experiments [70, 95] (such that  $r_{\text{exp}} = 0.68$  is around the upper value of  $r_{\text{exp}} = 0.52$  and the lower one for 0.75 within one standard deviation), we see that an uncertainty of at least 0.15 should be considered for the reference value of  $1 - W_{f_0}$ . The final

FIG. 2. The spectral density function  $\omega(E)$  is shown for the  $f_0(980)$  in the top panels and for the  $a_0(980)$  in the bottom ones. For the  $f_0(980)$  the poles considered are in the RS II, with the pole in Eq. (10) corresponding to the top left panel and the pole in Eq. (9) to the top right one. For the  $a_0(980)$  we take the poles in Eqs. (55) and (56), which are in the RS II (bottom left panel) and RS III (bottom right one), respectively. Every line in a plot corresponds to the indicated value of  $r_{\text{exp}}$  in the legends, and for the  $a_0(980)$  the poles lie in different RSs.

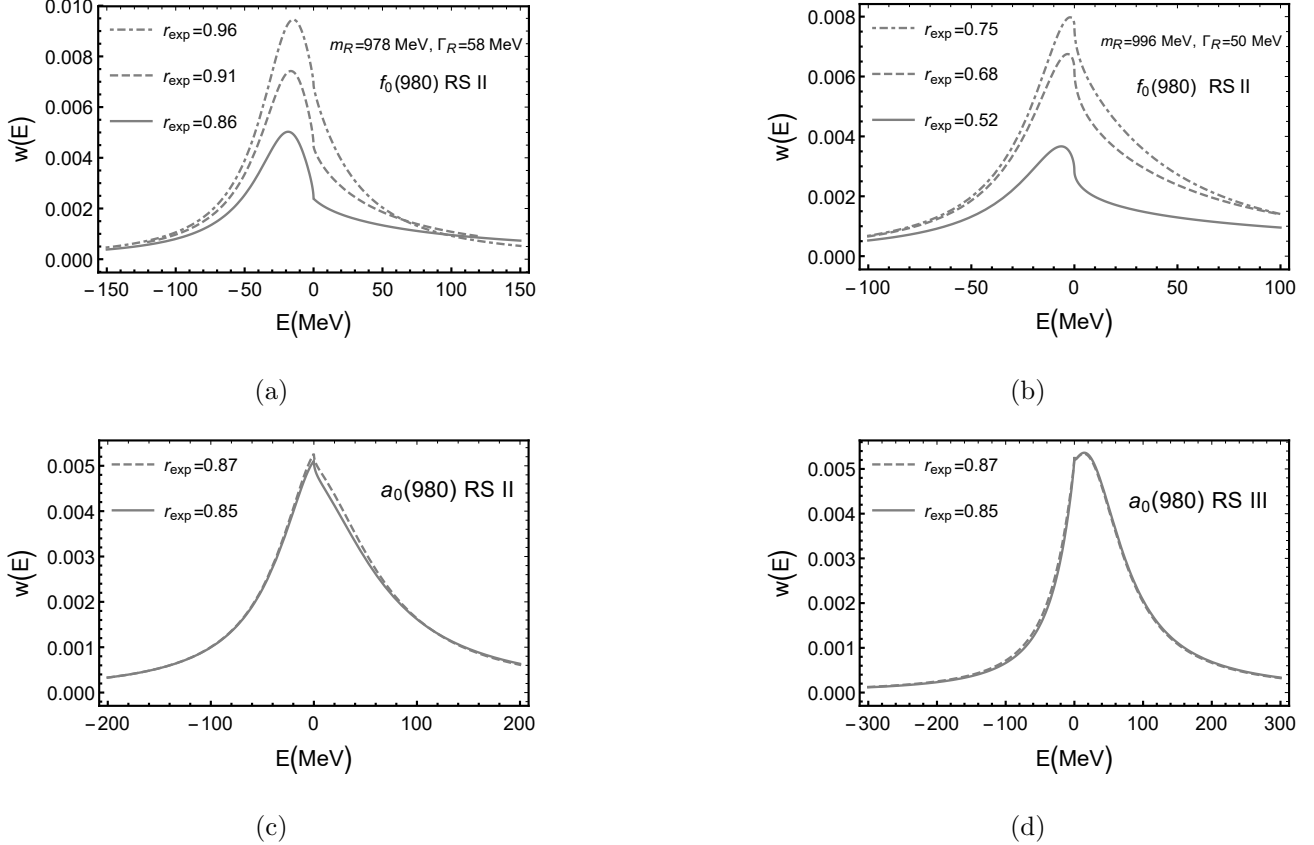


figure is given in the column before the last one in Table XII. We can appreciate that the central value obtained by integrating Eq. (47) is larger than the central value for  $X$  in Table VIII by employing Eq. (1), which is also given in the last column. Then, we would have  $1 - W_{f_0} = 0.76 \pm 0.15$  and  $0.50 \pm 0.15$  for  $r_{\text{exp}} = 0.52$  [70] and  $0.75$  [95], respectively, as also shown in Table XII. These figures indicate a dominant meson-meson component, mostly  $K\bar{K}$  ( $X_2 \gg X_1$ ), in the nature of the  $f_0(980)$  pole from Ref. [77], Eq. (9). It also follows that the results are compatible with those given for  $X$  within errors.

However, for  $r_{\text{exp}}$  from Ref. [95] the central value of  $1 - W_{f_0}$  in Table XII is only slightly above 0.5, and both values taken for  $r_{\text{exp}}$  [70, 95] generate values of  $1 - W_{f_0}$  that could decrease substantially once errors are taken into account. Therefore, other components apart from  $K\bar{K}$  are

TABLE XII. Resonance  $f_0(980)$  with the pole position in the RS II from Ref. [77], Eq. (9): We show the dependence of  $W_{f_0}$  on the integration interval  $[-\Delta, \Delta]$  with  $\Delta$  up to  $2\Gamma_R$ . For the experimental inputs of  $r_{\text{exp}}$  we give our final estimate for  $1 - W_{f_0}$  in the column 5. The total compositeness  $X = X_1 + X_2$  from Table VIII is given in the last column.

$r_{\text{exp}}$	$[-\Delta, \Delta]$	$W_{f_0}$	$(1 - W_{f_0})\Delta$	$1 - W_{f_0}$	$X$
0.52 [70]	$[-25, 25]$	0.13	0.87		
	$[-50, 50]$	0.21	0.79		
	$[-75, 75]$	0.27	0.73		
	$[-100, 100]$	0.31	0.69	$0.76 \pm 0.15$	$0.51 \pm 0.22$
0.68 [25]	$[-25, 25]$	0.25	0.75		
	$[-50, 50]$	0.39	0.61		
	$[-75, 75]$	0.47	0.53		
	$[-100, 100]$	0.53	0.47		$0.38 \pm 0.18$
0.75 [95]	$[-25, 25]$	0.30	0.70		
	$[-50, 50]$	0.45	0.55		
	$[-75, 75]$	0.55	0.45		
	$[-100, 100]$	0.61	0.39	$0.50 \pm 0.15$	$0.29 \pm 0.14$

likely to play a noticeable role in the composition of the  $f_0(980)$ . From non-perturbative studies based on unitarizing Chiral Perturbation Theory with/without resonances these extra components have been also unveiled [28, 74, 75, 96].

### B. The $a_0(980)$ resonance

Now, we follow similar steps and use the fact that the ratio of  $\Gamma(a_0(980) \rightarrow K\bar{K})/\Gamma(a_0(980) \rightarrow \pi\eta)$  is also given by Ref. [71], see Eqs. (55) and (56), with the values  $0.138 \pm 0.035$  (RS II) and  $0.149 \pm 0.039$  (RS III), respectively. The typical uncertainty for the inferred  $r_{\text{exp}}$  is around a 3%. We also consider the average value given by the PDG [49],  $\Gamma(a_0(980) \rightarrow K\bar{K})/\Gamma(a_0(980) \rightarrow \pi\eta) = 0.177 \pm 0.024$ , which implies an uncertainty of a 1.7% in  $r_{\text{exp}}$ .

Its implication has been organized in Table XIII, where we apply the method S with  $r_{\text{exp}}$  as input to the  $a_0(980)$  poles in the RS II and III. The  $K\bar{K}$  component is larger than the  $\pi\eta$  one, but the total compositeness  $X$  is small being less than 0.25 and 0.35 for for the RS II and III  $a_0(980)$

poles, respectively.

TABLE XIII. Method S applied to the resonance  $a_0(980)$  with pole positions from Ref. [71], Eqs. (55) and (56): By reproducing the input values of  $\Gamma_{a_0}$  and  $r_{\text{exp}}$  (column 2), we predict  $|\gamma_i|$  (columns 3, 4),  $\Gamma_i$  (columns 5, 6), and  $X_i$  (columns 7, 8).

$r_{\text{exp}}$	RS	$ \gamma_{\pi\eta} (\text{GeV})$	$ \gamma_{K\bar{K}} (\text{GeV})$	$\Gamma_1(\text{MeV})$	$\Gamma_2(\text{MeV})$	$X_{\pi\eta}$	$X_{K\bar{K}}$
0.85 [49]	II	$2.90 \pm 0.05$	$2.32 \pm 0.08$	$111.8 \pm 4.2$	$14.6 \pm 0.6$	$0.100 \pm 0.004$	$0.132 \pm 0.013$
	III	$2.86 \pm 0.05$	$2.61 \pm 0.72$	$108.0 \pm 3.7$	$19.1 \pm 0.7$	$0.098 \pm 0.004$	$0.249 \pm 0.017$
0.87 [71]	II	$2.88 \pm 0.05$	$2.16 \pm 0.07$	$109.8 \pm 4.2$	$12.6 \pm 0.5$	$0.098 \pm 0.004$	$0.115 \pm 0.009$
	III	$2.89 \pm 0.05$	$2.43 \pm 0.07$	$110.5 \pm 3.8$	$16.5 \pm 0.6$	$0.100 \pm 0.004$	$0.216 \pm 0.030$

TABLE XIV. Method F applied to the resonance  $a_0(980)$  with pole positions from Ref. [71], Eqs. (55) and (56): The branching ratio  $r_{\text{exp}}$  is taken as input (column 1), the RS in which the pole lies is indicated in the column 2. We then calculate the bare partial-decay width  $\tilde{\Gamma}_1$  (column 3), the bare coupling squared  $g_2$  (column 4),  $E_f$  (column 5), the renormalized  $\Gamma_1$  (column 6) and  $\Gamma_2$  (column 7), and the partial compositeness coefficients  $X_1$  (column 8) and  $X_2$  (column 9).

$r_{\text{exp}}$	RS	$\tilde{\Gamma}_{\pi\eta}(\text{MeV})$	$g_2$	$E_f(\text{MeV})$	$\Gamma_1(\text{MeV})$	$\Gamma_2(\text{MeV})$	$X_{\pi\eta}$	$X_{K\bar{K}}$
0.85 [49]	II	$124.0 \pm 5.3$	$0.21 \pm 0.03$	$3.08 \pm 5.11$	$111.8 \pm 4.2$	$14.6 \pm 0.6$	$0.100 \pm 0.004$	$0.116 \pm 0.017$
	III	$98.7 \pm 3.4$	$0.21 \pm 0.01$	$23.1 \pm 2.8$	$108.0 \pm 3.6$	$19.1 \pm 0.6$	$0.099 \pm 0.004$	$0.205 \pm 0.028$
0.87 [71]	II	$119.9 \pm 4.9$	$0.18 \pm 0.02$	$4.65 \pm 4.82$	$109.8 \pm 4.2$	$12.6 \pm 0.5$	$0.098 \pm 0.004$	$0.100 \pm 0.016$
	III	$102.0 \pm 3.5$	$0.18 \pm 0.01$	$21.6 \pm 2.9$	$110.5 \pm 3.7$	$16.5 \pm 0.6$	$0.101 \pm 0.004$	$0.178 \pm 0.038$

We now proceed with the application of the method F with  $r_{\text{exp}}$  as input and the results obtained are presented in Table XIV. We observe that the values of  $X_2$  and  $\Gamma_{K\bar{K}}$  are rather similar between Tables VI and XIV, and similarly if we compare the latter with Table XIII where  $r_{\text{exp}}$  is taken as input too. Thus, we find compatibility between different methods for the  $a_0(980)$  case. It is also clear from Table XIV that the value of  $r_{\text{exp}} = 0.85$  obtained from the PDG average value of  $\Gamma(a_0(980) \rightarrow K\bar{K})/\Gamma(a_0(980) \rightarrow \pi\eta) = 0.177 \pm 0.024$  [49] implies quite small values for  $X_2 \lesssim 0.3$ .

It seems in our opinion that an uncertainty of only 2 – 3% in  $r_{\text{exp}}$  for the  $a_0(980)$  is probably too optimistic. In this respect we notice that the analysis of Ref. [71] for the  $a_0(980)$  is based on taking poles in the RS II and III for this resonance, while recent sophisticated theoretical studies

[72, 73], which also reproduce lattice QCD data, require a very different qualitative picture with a pole in the RS IV. In this respect, let us check the sensitivity of the results based on Eq. (1) for the calculation of  $X$ , and for that take e.g. the  $a_0(980)$  pole in the RS II and  $r_{\text{exp}} = 0.85 \pm 0.15$ , which corresponds to the average value of the PDG with an ad-hoc uncertainty of around a 20%. We indeed find a strong sensitivity, such that for the central value  $r_{\text{exp}} = 0.85$  we have the values for the couplings  $|\gamma_1| = 2.9$  GeV and  $|\gamma_2| = 2.2$  GeV, while for the lower end  $r_{\text{exp}} = 0.85 - 0.15 = 0.70$  we find a new solution with the values  $|\gamma_1| = 3.1$  GeV and  $|\gamma_2| = 3.2$  GeV. With respect to the central value we have a variation of only a 6% in  $|\gamma_1|$ , but  $|\gamma_2|$  is now a 44% bigger (a factor of 2 for the square of the coupling). The variation is of similar size if considering  $r_{\text{exp}} = 0.87 \pm 0.17$  with the central value from Ref. [71] and an ad-hoc 20% uncertainty taken.

Thus, it is advisable to also apply for the  $a_0(980)$  case the method based on the spectral density function (which is less sensitive to small variations in the input value for  $r_{\text{exp}}$ ) and evaluate the compositeness  $1 - W_{a_0}$  as a function of  $\Delta$ . We give the results in Tables XV and XVI for the  $a_0(980)$  poles in the RS II, Eq. (55), and RS III, Eq. (56), respectively. The dependence with  $\Delta$  is indicated by the subscript  $\Delta$  in the fourth column,  $(1 - W_{a_0})_\Delta$ . Taking into account the variation in the value of  $1 - W_{f_0}$  between  $\Delta \approx \Gamma_{a_0}$  and  $\Delta \approx 1.5\Gamma_{a_0}$ , we give our range of values calculated for  $1 - W_{a_0}$  in the column before the last one in Tables XV and XVI. The output is similar in both tables with values for  $1 - W_{a_0}$  typically within the range 0.3 – 0.4. When compared with  $X$  from Table XIV, given in the last column in Tables XV and XVI, we see a quantitative agreement in the case of the RS III pole, and a semiquantitative one for the RS II one. The emerging picture is that  $X$  is clearly less than 0.5, ranging between 0.2 – 0.4 depending on the method of calculation. Therefore, other components beyond  $\pi\eta$  and  $K\bar{K}$  are also required [37, 38]. However, if the resonance lied in RS IV, as preferred by the recent analyses [72, 73], our approach does not apply and we cannot extend such conclusion to that case.

TABLE XV. Resonance  $a_0(980)$  with the pole position in the RS II from Ref. [71], Eq. (55). The dependence of  $W_{a_0}$  on the integration interval  $[-\Delta, \Delta]$  for the  $a_0(980)$  is shown with  $\Delta$  up to  $2\Gamma_{a_0}$ . In the column 5 we provide our interval estimated for  $1 - W_{a_0}$  and in the last one  $X = X_1 + X_2$  from Table XIV is given.

$r_{\text{exp}}$	$[-\Delta, \Delta]$	$W_{a_0}$	$(1 - W_{a_0})_{\Delta}$	$1 - W_{a_0}$	$X$
0.85 [49]	$[-50, 50]$	0.38	0.62		
	$[-100, 100]$	0.57	0.43		
	$[-150, 150]$	0.67	0.33		
	$[-200, 200]$	0.73	0.27	0.33 – 0.43	$0.216 \pm 0.017$
0.87 [71]	$[-50, 50]$	0.39	0.61		
	$[-100, 100]$	0.59	0.41		
	$[-150, 150]$	0.68	0.32		
	$[-200, 200]$	0.74	0.26	0.32 – 0.41	$0.198 \pm 0.016$

TABLE XVI. Resonance  $a_0(980)$  with the pole position in the RS III from Ref. [71], Eq. (56). The dependence of  $W_{a_0}$  on the integration interval  $[-\Delta, \Delta]$  for the  $a_0(980)$  is shown with  $\Delta$  up to  $2\Gamma_{a_0}$ . In the column 5 we provide our interval estimated for  $1 - W_{a_0}$  and in the last one  $X = X_1 + X_2$  from Table XIV is given.

$r_{\text{exp}}$	$[-\Delta, \Delta]$	$W_{a_0}$	$(1 - W_{a_0})_{\Delta}$	$1 - W_{a_0}$	$X$
0.85 [49]	$[-50, 50]$	0.39	0.61		
	$[-100, 100]$	0.59	0.41		
	$[-150, 150]$	0.69	0.31		
	$[-200, 200]$	0.75	0.25		
	$[-250, 250]$	0.79	0.21	0.31 – 0.41	$0.303 \pm 0.030$
0.87 [71]	$[-50, 50]$	0.40	0.60		
	$[-100, 100]$	0.60	0.40		
	$[-150, 150]$	0.70	0.30		
	$[-200, 200]$	0.76	0.24		
	$[-250, 250]$	0.80	0.20	0.30 – 0.40	$0.279 \pm 0.037$

We would also like to comment about the clearly visible cusp effect for most of the curves of

$\omega(E)$  in Fig. 2. This change in the shape of  $\omega(E)$  below and above the two-kaon threshold is due to the fact that if the resonance pole lies in the RS II (III) then there is no associated pole in the RS III (II) above (below) the  $K\bar{K}$  threshold. Precisely the RS III (II) is the one that connects with the physical region there.

## VI. SUMMARY AND CONCLUSIONS

This paper discusses the importance of the continuum channels  $\pi\pi-K\bar{K}$  and  $\pi\eta-K\bar{K}$  in the composition of the  $f_0(980)$  and  $a_0(980)$  resonances, which is quantified by the concept of the total compositeness  $X$ . In our calculation we exploit the tight relationship between the compositeness  $X$ , the mass and the decay width of a resonance. The threshold of the  $K\bar{K}$  pair is very close to the mass of each resonance and this fact has main consequences in our results. We develop two methods: One is based on saturating the total width and compositeness; the other relies on the use of a Flatté parameterization and, in some instances, of the spectral function of a near-threshold resonance.

We provide input values for the mass and width of each resonance by taking their pole positions from relevant analyses in the literature. Regarding the third input needed in our analyses we first take input values for  $X$  in the compositeness relationship and we predict the couplings, partial compositeness coefficients and partial-decay widths to the  $\pi\pi$  ( $\pi\eta$ ) and  $K\bar{K}$  channels for the  $f_0(980)$  ( $a_0(980)$ ). There is an interesting trend in the results such that the larger  $X$ , the smaller the branching decay ratio to the lighter channel,  $r_{\text{exp}}$ . This is due to the increase of the coupling to the heavier  $K\bar{K}$  channel with increasing  $X$ , compensating the reduced phase space available for the decay of the resonances into this channel. It is also found that for the  $f_0(980)$  the partial compositeness coefficient of  $K\bar{K}$ ,  $X_2$ , is larger by orders of magnitude than the corresponding one to  $\pi\pi$ ,  $X_1$ . For the  $a_0(980)$  the compositeness for  $K\bar{K}$  is also larger than the one associated to  $\pi\eta$ , but as  $X$  decreases they tend to become similar in size.

Another possibility is to replace the third input  $X$  by reported values in the literature for  $r_{\text{exp}}$ . However, if  $X_2$  is calculated in terms of the coupling squared to  $K\bar{K}$  and the derivative of the unitary-loop function in the corresponding Riemann sheet, we typically find a large sensitivity on the input value for  $r_{\text{exp}}$ . The situation is improved when using the method based on integrating the spectral density function around the  $K\bar{K}$  threshold along the energy region comprising the resonance signal, so that more stable results are obtained under small changes in  $r_{\text{exp}}$ . It turns out that for the poles considered the meson-meson components are dominant for the  $f_0(980)$ , while for the  $a_0(980)$  they are subdominant.

Throughout the manuscript we have emphasized the need to distinguish in a Flatté parameterization between the bare couplings/widths, on the one hand, and the dressed/renormalized ones, on the other hand. We have also shown how to calculate the latter ones. In addition, we discuss the relationship between the partial-decay widths directly calculated in terms of the dressed couplings and the actually measured ones. In this regard, we show the changes needed for a pole in the second Riemann sheet lying near the heavier threshold, such that the total width is then  $\Gamma_R = \Gamma_1 - \Gamma_2$ , instead of the standard  $\Gamma_R = \Gamma_1 + \Gamma_2$  for a pole in the third Riemann sheet.

Finally, we stress that the compositeness concept, as a quantitative examination of the inner structure of a resonance/molecule, is a relevant tool to promote a step forward in the understanding of the structure of a hadronic state.

### ACKNOWLEDGMENTS

We would like to thank useful discussions with Zhi-Hui Guo, J. R. Peláez and J. Ruiz de Elvira. The author XWK is supported by the National Natural Science Foundation of China (NSFC) under Project No. 11805012. JAO acknowledges partial financial support by the MICINN AEI (Spain) Grant No. PID2019-106080GB-C22/AEI/10.13039/501100011033, and by the EU Horizon 2020 research and innovation programme, STRONG-2020 project, under grant agreement No. 824093.

- 
- [1] S. D. Protopopescu, M. Alston-Garnjost, A. Barbaro-Galtieri, S. M. Flatte, J. H. Friedman, T. A. Lasinski, G. R. Lynch, M. S. Rabin, and F. T. Solmitz, *Phys. Rev. D* **7**, 1279 (1973).
  - [2] R. Ammar, R. Davis, W. Kropac, J. Mott, D. Slate, B. Werner, M. Derrick, T. Fields, and F. Schweingruber, *Phys. Rev. Lett.* **21**, 1832 (1968).
  - [3] R. L. Jaffe, *Phys. Rev. D* **15**, 267 (1977).
  - [4] R. L. Jaffe, *Phys. Rev. D* **15**, 281 (1977).
  - [5] E. van Beveren, T. A. Rijken, K. Metzger, C. Dullemond, G. Rupp, and J. E. Ribeiro, *Z. Phys. C* **30**, 615 (1986), [arXiv:0710.4067 \[hep-ph\]](#).
  - [6] M. Napsuciale, (1998), [arXiv:hep-ph/9803396](#).
  - [7] D. Black, A. H. Fariborz, S. Moussa, S. Nasri, and J. Schechter, *Phys. Rev. D* **64**, 014031 (2001), [arXiv:hep-ph/0012278](#).
  - [8] J. A. Oller, *Nucl. Phys. A* **727**, 353 (2003), [arXiv:hep-ph/0306031](#).
  - [9] B. Moussallam, *Eur. Phys. J. C* **71**, 1814 (2011), [arXiv:1110.6074 \[hep-ph\]](#).

- [10] B. Moussallam, *Eur. Phys. J. C* **14**, 111 (2000), [arXiv:hep-ph/9909292](#).
- [11] J. A. Oller and L. Roca, *Eur. Phys. J. A* **34**, 371 (2007), [arXiv:hep-ph/0608290](#).
- [12] J. A. Oller and L. Roca, *Phys. Lett. B* **651**, 139 (2007), [arXiv:0704.0039 \[hep-ph\]](#).
- [13] M. Albaladejo, J. A. Oller, and L. Roca, *Phys. Rev. D* **82**, 094019 (2010), [arXiv:1011.1434 \[hep-ph\]](#).
- [14] L. Alvarez-Ruso, J. A. Oller, and J. M. Alarcon, *Phys. Rev. D* **80**, 054011 (2009), [arXiv:0906.0222 \[hep-ph\]](#).
- [15] L. Alvarez-Ruso, J. A. Oller, and J. M. Alarcon, *Phys. Rev. D* **82**, 094028 (2010), [arXiv:1007.4512 \[hep-ph\]](#).
- [16] N. N. Achasov, S. A. Devyanin, and G. N. Shestakov, *Phys. Lett. B* **96**, 168 (1980).
- [17] N. N. Achasov, *Nucl. Phys. A* **675**, 279C (2000), [arXiv:hep-ph/9910540](#).
- [18] N. N. Achasov, J. V. Bennett, A. V. Kiselev, E. A. Kozyrev, and G. N. Shestakov, *Phys. Rev. D* **103**, 014010 (2021), [arXiv:2009.04191 \[hep-ph\]](#).
- [19] J. Vijande and A. Valcarce, *Symmetry* **1**, 155 (2009), [arXiv:0912.3605 \[hep-ph\]](#).
- [20] J. D. Weinstein and N. Isgur, *Phys. Rev. Lett.* **48**, 659 (1982).
- [21] J. D. Weinstein and N. Isgur, *Phys. Rev. D* **27**, 588 (1983).
- [22] H. A. Ahmed and C. W. Xiao, *Phys. Rev. D* **101**, 094034 (2020), [arXiv:2001.08141 \[hep-ph\]](#).
- [23] L.-Y. Dai and M. R. Pennington, *Phys. Rev. D* **90**, 036004 (2014), [arXiv:1404.7524 \[hep-ph\]](#).
- [24] L. Y. Dai, X. G. Wang, and H. Q. Zheng, *Commun. Theor. Phys.* **57**, 841 (2012), [arXiv:1108.1451 \[hep-ph\]](#).
- [25] J. A. Oller and E. Oset, *Nucl. Phys. A* **620**, 438 (1997), [Erratum: *Nucl.Phys.A* 652, 407–409 (1999)], [arXiv:hep-ph/9702314](#).
- [26] J. A. Oller, E. Oset, and J. R. Pelaez, *Phys. Rev. Lett.* **80**, 3452 (1998), [arXiv:hep-ph/9803242](#).
- [27] J. A. Oller, E. Oset, and J. R. Pelaez, *Phys. Rev. D* **59**, 074001 (1999), [Erratum: *Phys.Rev.D* 60, 099906 (1999), Erratum: *Phys.Rev.D* 75, 099903 (2007)], [arXiv:hep-ph/9804209](#).
- [28] J. A. Oller and E. Oset, *Phys. Rev. D* **60**, 074023 (1999), [arXiv:hep-ph/9809337](#).
- [29] G. Janssen, B. C. Pearce, K. Holinde, and J. Speth, *Phys. Rev. D* **52**, 2690 (1995), [arXiv:nucl-th/9411021](#).
- [30] D. Lohse, J. W. Durso, K. Holinde, and J. Speth, *Nucl. Phys. A* **516**, 513 (1990).
- [31] A. Bramon and E. Masso, *Phys. Lett. B* **93**, 65 (1980), [Erratum: *Phys.Lett.B* 107, 455 (1981)].
- [32] N. A. Tornqvist, *Z. Phys. C* **68**, 647 (1995), [arXiv:hep-ph/9504372](#).
- [33] D. Black, A. H. Fariborz, F. Sannino, and J. Schechter, *Phys. Rev. D* **59**, 074026 (1999), [arXiv:hep-ph/9808415](#).
- [34] M. D. Scadron, *Eur. Phys. J. C* **6**, 141 (1999), [arXiv:hep-ph/9710317](#).

- [35] M. Napsuciale and S. Rodriguez, *Phys. Lett. B* **603**, 195 (2004), [arXiv:hep-ph/0403072](#).
- [36] M. Napsuciale and S. Rodriguez, *Phys. Rev. D* **70**, 094043 (2004), [arXiv:hep-ph/0407037](#).
- [37] L.-Y. Dai, X.-G. Wang, and H.-Q. Zheng, *Commun. Theor. Phys.* **58**, 410 (2012), [arXiv:1206.5481 \[hep-ph\]](#).
- [38] T. Sekihara and S. Kumano, *Phys. Rev. D* **92**, 034010 (2015), [arXiv:1409.2213 \[hep-ph\]](#).
- [39] N. N. Achasov, S. A. Devyanin, and G. N. Shestakov, *Phys. Lett. B* **88**, 367 (1979).
- [40] A. E. Kudryavtsev, V. E. Tarasov, J. Haidenbauer, C. Hanhart, and J. Speth, *Phys. Rev. C* **66**, 015207 (2002), [arXiv:nucl-th/0203034](#).
- [41] C. Hanhart, B. Kubis, and J. R. Pelaez, *Phys. Rev. D* **76**, 074028 (2007), [arXiv:0707.0262 \[hep-ph\]](#).
- [42] J. A. Oller, E. Oset, and J. R. Pelaez, *Phys. Rev. D* **62**, 114017 (2000), [arXiv:hep-ph/9911297](#).
- [43] H.-Y. Cheng and X.-W. Kang, *Eur. Phys. J. C* **77**, 587 (2017), [Erratum: *Eur.Phys.J.C* 77, 863 (2017)], [arXiv:1707.02851 \[hep-ph\]](#).
- [44] X.-W. Kang, T. Luo, Y. Zhang, L.-Y. Dai, and C. Wang, *Eur. Phys. J. C* **78**, 909 (2018), [arXiv:1808.02432 \[hep-ph\]](#).
- [45] X.-W. Kang, B. Kubis, C. Hanhart, and U.-G. Meißner, *Phys. Rev. D* **89**, 053015 (2014), [arXiv:1312.1193 \[hep-ph\]](#).
- [46] F. E. Close and N. A. Tornqvist, *J. Phys. G* **28**, R249 (2002), [arXiv:hep-ph/0204205](#).
- [47] E. Klempt and A. Zaitsev, *Phys. Rept.* **454**, 1 (2007), [arXiv:0708.4016 \[hep-ph\]](#).
- [48] D.-L. Yao, L.-Y. Dai, H.-Q. Zheng, and Z.-Y. Zhou, (2020), [arXiv:2009.13495 \[hep-ph\]](#).
- [49] P. A. Zyla *et al.* (Particle Data Group), *PTEP* **2020**, 083C01 (2020).
- [50] T. Cohen, F. J. Llanes-Estrada, J. R. Pelaez, and J. Ruiz de Elvira, *Phys. Rev. D* **90**, 036003 (2014), [arXiv:1405.4831 \[hep-ph\]](#).
- [51] G. 't Hooft, G. Isidori, L. Maiani, A. D. Polosa, and V. Riquer, *Phys. Lett. B* **662**, 424 (2008), [arXiv:0801.2288 \[hep-ph\]](#).
- [52] S. Narison, *Nucl. Phys. B Proc. Suppl.* **96**, 244 (2001), [arXiv:hep-ph/0012235](#).
- [53] S. Weinberg, *Phys. Rev.* **130**, 776 (1963).
- [54] J. A. Oller, *Annals Phys.* **396**, 429 (2018), [arXiv:1710.00991 \[hep-ph\]](#).
- [55] V. Baru, J. Haidenbauer, C. Hanhart, Y. Kalashnikova, and A. E. Kudryavtsev, *Phys. Lett. B* **586**, 53 (2004), [arXiv:hep-ph/0308129](#).
- [56] T. Hyodo, D. Jido, and A. Hosaka, *Phys. Rev. C* **85**, 015201 (2012), [arXiv:1108.5524 \[nucl-th\]](#).
- [57] F. Aceti and E. Oset, *Phys. Rev. D* **86**, 014012 (2012), [arXiv:1202.4607 \[hep-ph\]](#).
- [58] F. Aceti, L. R. Dai, L. S. Geng, E. Oset, and Y. Zhang, *Eur. Phys. J. A* **50**, 57 (2014), [arXiv:1301.2554 \[hep-ph\]](#).

- [59] T. Sekihara, T. Hyodo, and D. Jido, *PTEP* **2015**, 063D04 (2015), arXiv:1411.2308 [hep-ph].
- [60] I. Matuschek, V. Baru, F.-K. Guo, and C. Hanhart, *Eur. Phys. J. A* **57**, 101 (2021), arXiv:2007.05329 [hep-ph].
- [61] Z.-H. Guo and J. A. Oller, *Phys. Rev. D* **93**, 096001 (2016), arXiv:1508.06400 [hep-ph].
- [62] U.-G. Meißner and J. A. Oller, *Phys. Lett. B* **751**, 59 (2015), arXiv:1507.07478 [hep-ph].
- [63] X.-W. Kang, Z.-H. Guo, and J. A. Oller, *Phys. Rev. D* **94**, 014012 (2016), arXiv:1603.05546 [hep-ph].
- [64] X.-W. Kang and J. A. Oller, *Eur. Phys. J. C* **77**, 399 (2017), arXiv:1612.08420 [hep-ph].
- [65] R. Gao, Z.-H. Guo, X.-W. Kang, and J. A. Oller, *Adv. High Energy Phys.* **2019**, 4651908 (2019), arXiv:1812.07323 [hep-ph].
- [66] Z.-H. Guo and J. A. Oller, *Phys. Rev. D* **103**, 054021 (2021), arXiv:2012.11904 [hep-ph].
- [67] Z.-H. Guo and J. A. Oller, *Phys. Rev. D* **103**, 034024 (2021), arXiv:2011.00978 [hep-ph].
- [68] M.-L. Du, Z.-H. Guo, and J. A. Oller, (2021), arXiv:2109.14237 [hep-ph].
- [69] L. N. Bogdanova, G. M. Hale, and V. E. Markushin, *Phys. Rev. C* **44**, 1289 (1991).
- [70] B. Aubert *et al.* (BaBar), *Phys. Rev. D* **74**, 032003 (2006), arXiv:hep-ex/0605003.
- [71] M. Albrecht *et al.* (Crystal Barrel), *Eur. Phys. J. C* **80**, 453 (2020), arXiv:1909.07091 [hep-ex].
- [72] Z.-H. Guo, L. Liu, U.-G. Meißner, J. A. Oller, and A. Rusetsky, *Phys. Rev. D* **95**, 054004 (2017), arXiv:1609.08096 [hep-ph].
- [73] J. J. Dudek, R. G. Edwards, and D. J. Wilson (Hadron Spectrum), *Phys. Rev. D* **93**, 094506 (2016), arXiv:1602.05122 [hep-ph].
- [74] Z.-H. Guo, J. A. Oller, and J. Ruiz de Elvira, *Phys. Rev. D* **86**, 054006 (2012), arXiv:1206.4163 [hep-ph].
- [75] Z.-H. Guo, J. A. Oller, and J. Ruiz de Elvira, *Phys. Lett. B* **712**, 407 (2012), arXiv:1203.4381 [hep-ph].
- [76] A. Salam, *Nuovo Cim.* **25**, 224 (1962).
- [77] R. Garcia-Martin, R. Kaminski, J. R. Pelaez, and J. Ruiz de Elvira, *Phys. Rev. Lett.* **107**, 072001 (2011), arXiv:1107.1635 [hep-ph].
- [78] R. Garcia-Martin, R. Kaminski, J. R. Pelaez, J. Ruiz de Elvira, and F. J. Yndurain, *Phys. Rev. D* **83**, 074004 (2011), arXiv:1102.2183 [hep-ph].
- [79] P. Di Vecchia and G. Veneziano, *Nucl. Phys. B* **171**, 253 (1980).
- [80] C. Rosenzweig, J. Schechter, and C. G. Trahern, *Phys. Rev. D* **21**, 3388 (1980).
- [81] E. Witten, *Annals Phys.* **128**, 363 (1980).
- [82] K. Kawarabayashi and N. Ohta, *Nucl. Phys. B* **175**, 477 (1980).
- [83] K. Kawarabayashi and N. Ohta, *Prog. Theor. Phys.* **66**, 1789 (1981).

- [84] R. Kaiser and H. Leutwyler, *Eur. Phys. J. C* **17**, 623 (2000), arXiv:hep-ph/0007101.
- [85] P. Herrera-Siklody, J. I. Latorre, P. Pascual, and J. Taron, *Nucl. Phys. B* **497**, 345 (1997), arXiv:hep-ph/9610549.
- [86] M. Albaladejo and J. A. Oller, *Phys. Rev. Lett.* **101**, 252002 (2008), arXiv:0801.4929 [hep-ph].
- [87] A. Salas-Bernárdez, F. J. Llanes-Estrada, J. Escudero-Pedrosa, and J. A. Oller, *SciPost Phys.* **11**, 020 (2021), arXiv:2010.13709 [hep-ph].
- [88] J. A. Oller, L. Roca, and C. Schat, *Phys. Lett. B* **659**, 201 (2008), arXiv:0708.1659 [hep-ph].
- [89] J. A. Oller and L. Roca, *Eur. Phys. J. A* **37**, 15 (2008), arXiv:0804.0309 [hep-ph].
- [90] J. M. Dias, G. Toledo, L. Roca, and E. Oset, *Phys. Rev. D* **103**, 116019 (2021), arXiv:2102.08402 [hep-ph].
- [91] S. M. Flatte, *Phys. Lett. B* **63**, 224 (1976).
- [92] V. Baru, C. Hanhart, Y. S. Kalashnikova, A. E. Kudryavtsev, and A. V. Nefediev, *Eur. Phys. J. A* **44**, 93 (2010), arXiv:1001.0369 [hep-ph].
- [93] Z.-H. Guo and J. A. Oller, *Phys. Lett. B* **793**, 144 (2019), arXiv:1904.00851 [hep-ph].
- [94] Z.-H. Guo and J. A. Oller, *Phys. Rev. D* **84**, 034005 (2011), arXiv:1104.2849 [hep-ph].
- [95] M. Ablikim *et al.* (BES), *Phys. Rev. D* **72**, 092002 (2005), arXiv:hep-ex/0508050.
- [96] J. R. Pelaez and G. Rios, *Phys. Rev. Lett.* **97**, 242002 (2006), arXiv:hep-ph/0610397.